Atmos. Chem. Phys., 15, 7497–7522, 2015
www.atmos-chem-phys.net/15/7497/2015/
doi:10.5194/acp-15-7497-2015

Atmospheric Chemistry and Physics
Open Access

Secondary organic aerosol formation from the β-pinene+NO_3 system: effect of humidity and peroxy radical fate

C. M. Boyd[1], J. Sanchez[1], L. Xu[1], A. J. Eugene[2], T. Nah[1], W. Y. Tuet[1], M. I. Guzman[2], and N. L. Ng[1,3]

[1]School of Chemical and Biomolecular Engineering, Georgia Institute of Technology, Atlanta, GA 30332, USA
[2]Department of Chemistry, University of Kentucky, Lexington, KY 40506, USA
[3]School of Earth and Atmospheric Sciences, Georgia Institute of Technology, Atlanta, GA 30332, USA

Correspondence to: N. L. Ng (ng@chbe.gatech.edu)

Received: 23 December 2014 – Published in Atmos. Chem. Phys. Discuss.: 28 January 2015
Revised: 28 January 2015 – Accepted: 10 June 2015 – Published: 10 July 2015

Abstract. The formation of secondary organic aerosol (SOA) from the oxidation of β-pinene via nitrate radicals is investigated in the Georgia Tech Environmental Chamber (GTEC) facility. Aerosol yields are determined for experiments performed under both dry (relative humidity (RH) $< 2\,\%$) and humid (RH $= 50\,\%$ and RH $= 70\,\%$) conditions. To probe the effects of peroxy radical (RO_2) fate on aerosol formation, "RO_2+NO_3 dominant" and "RO_2+HO_2 dominant" experiments are performed. Gas-phase organic nitrate species (with molecular weights of 215, 229, 231, and 245 amu, which likely correspond to molecular formulas of $C_{10}H_{17}NO_4$, $C_{10}H_{15}NO_5$, $C_{10}H_{17}NO_5$, and $C_{10}H_{15}NO_6$, respectively) are detected by chemical ionization mass spectrometry (CIMS) and their formation mechanisms are proposed. The NO^+ (at m/z 30) and NO_2^+ (at m/z 46) ions contribute about 11 % to the combined organics and nitrate signals in the typical aerosol mass spectrum, with the $NO^+ : NO_2^+$ ratio ranging from 4.8 to 10.2 in all experiments conducted. The SOA yields in the "RO_2+NO_3 dominant" and "RO_2+HO_2 dominant" experiments are comparable. For a wide range of organic mass loadings (5.1–216.1 $\mu g\,m^{-3}$), the aerosol mass yield is calculated to be 27.0–104.1 %. Although humidity does not appear to affect SOA yields, there is evidence of particle-phase hydrolysis of organic nitrates, which are estimated to compose 45–74 % of the organic aerosol. The extent of organic nitrate hydrolysis is significantl lower than that observed in previous studies on photooxidation of volatile organic compounds in the presence of NO_x. It is estimated that about 90 and 10 % of the organic nitrates formed from the β-pinene+NO_3 reaction are primary organic nitrates and tertiary organic nitrates, respectively. While the primary organic nitrates do not appear to hydrolyze, the tertiary organic nitrates undergo hydrolysis with a lifetime of 3–4.5 h. Results from this laboratory chamber study provide the fundamental data to evaluate the contributions of monoterpene+NO_3 reaction to ambient organic aerosol measured in the southeastern United States, including the Southern Oxidant and Aerosol Study (SOAS) and the Southeastern Center for Air Pollution and Epidemiology (SCAPE) study.

1 Introduction

Owing to their high emissions and high reactivity with the major atmospheric oxidants (O_3, OH, NO_3), the oxidation of biogenic volatile organic compounds (BVOCs) emitted by vegetation, such as isoprene (C_5H_8), monoterpenes ($C_{10}H_{16}$), and sesquiterpenes ($C_{15}H_{24}$), is believed to be the dominant contributor to global secondary organic aerosol (SOA) formation (e.g., Kanakidou et al., 2005). While this is supported by the observation that ambient organic aerosol is predominantly "modern" and therefore biogenic in origin (Lewis et al., 2004; Schichtel et al., 2008; Marley et al., 2009), there exists an apparent contradiction because ambient organic aerosol is well correlated with anthropogenic tracers (de Gouw et al., 2005; Weber et al., 2007). This apparent discrepancy could be reconciled if anthropogenic pollution influence the atmospheric oxidation of BVOCs and their aerosol formation pathways. The oxidation of BVOCs by nitrate radicals (NO_3), formed from the reaction of ozone with NO_2, provides a direct link between anthropogenic pol-

lution and the abundance of biogenic carbon in atmospheric aerosol.

Biogenic hydrocarbons react rapidly with nitrate radicals (Atkinson and Arey, 2003a) and the SOA yields are generally higher than in photooxidation and ozonolysis (e.g., Griffi et al., 1999; Hallquist et al., 1999; Spittler et al., 2006; Ng et al., 2008; Fry et al., 2009, 2011, 2014; Rollins et al., 2009). As monoterpene emissions are not entirely light dependent, they are emitted during the day and at night (Fuentes et al., 2000; Guenther et al., 2012) and can contribute substantially to ambient organic aerosol. Monoterpenes have also been found to make up as much as 28 % of non-methane organic carbon emissions from biomass burning in both fiel and laboratory studies (Akagi et al., 2013; Hatch et al., 2015; Stockwell et al., 2015). Fires from biomass burning are more likely to smolder at night and are therefore more likely to emit monoterpenes, which can then react with nitrate radicals (Akagi et al., 2013). Results from previous fiel studies provided evidence of aerosol formation from nitrate radical oxidation of BVOCs during both daytime and nighttime (McLaren et al., 2004; Iinuma et al., 2007; Fuentes et al., 2007; Brown et al., 2009, 2013; Rastogi et al., 2011; Rollins et al., 2012; Rollins et al., 2013). Specifi ally, many of these studies found a significan increase in the amount of monoterpene organic aerosol and oxidation products at night, which could be attributed to nighttime monoterpene oxidation by nitrate radicals (McLaren et al., 2004; Iinuma et al., 2007; Rastogi et al., 2011). Results from recent fligh measurements in Houston, TX, also showed that organic aerosol was enhanced in the nocturnal boundary layer at levels in excess of those attributable to primary emissions, implying a source of SOA from the BVOCs+NO_3 reaction (Brown et al., 2013).

Global modeling studies showed large variations in the total SOA burden that can be attributed to the oxidation of BVOCs by nitrate radicals, ranging from $\sim$ 5 to 21 % (Hoyle et al., 2007; Pye et al., 2010). Specificall , Pye et al. (2010) showed that the inclusion of nitrate radical oxidation reaction doubled the total amount of terpene (monoterpenes and sesquiterpenes) aerosol, pointing to the significan contribution of this chemistry to total organic aerosol burden. In these modeling studies, all aerosol formation from the nitrate radical oxidation of terpenes was calculated based on the β-pinene+NO_3 SOA yields obtained in Griffi et al. (1999). A recent modeling study by Russell and Allen (2005) determined that as much as 20 % of all nighttime SOA is from the reaction of β-pinene+NO_3. Due to the significanc of nitrate radical oxidation pathways in SOA formation, it is important that the SOA yields for BVOCs+NO_3, and especially that of β-pinene+NO_3, are well constrained from fundamental laboratory studies and accurately represented in models.

The majority of the previous laboratory studies of the BVOCs+NO_3 chemistry were performed under dry conditions (Berndt and Boge, 1997a, b; Wängberg et al., 1997; Griffi et al., 1999; Hallquist et al., 1999; Bonn and Moorgat, 2002; Spittler et al., 2006; Ng et al., 2008; Rollins et al., 2009; Fry et al., 2009, 2011, 2014; Perraud et al., 2010; Kwan et al., 2012; Jaoui et al., 2013). The effect of relative humidity on SOA formation, however, could potentially be important for nighttime (where NO_3 radicals dominate) and early morning chemistry as the ambient relative humidity (RH) is typically higher at these times. Several recent studies have investigated the effect of water on SOA formation from the nitrate radical oxidation pathways but the results are inconclusive. For instance, Spittler et al. (2006) found that the SOA yield is lower at 20 % RH compared to dry conditions, suggesting that water vapor may alter the gas-phase oxidation mechanism and/or partitioning into the particle phase, thus shifting the equilibrium partitioning of organic compounds. However, other studies showed that the presence of water vapor did not affect particle size distributions and SOA formation (Bonn and Moorgat, 2002; Fry et al., 2009). Thus, the role of water in SOA formation from nitrate radical oxidation of BVOCs is still unclear.

Another important parameter in SOA formation from BVOCs+NO_3 is the fate of peroxy radicals, which directly determines the oxidation products, SOA yields, and aerosol chemical and physical properties (Kroll and Seinfeld, 2008; Orlando and Tyndall, 2012; Ziemann and Atkinson, 2012). Previous studies regarding the effects of peroxy radical fates on SOA formation from BVOCs typically focused on photooxidation and ozonolysis systems (e.g., Presto et al., 2005; Kroll et al., 2006; Ng et al., 2007a; Eddingsaas et al., 2012; Xu et al., 2014) and isoprene+NO_3 chemistry (Kwan et al., 2012; Ng et al., 2008; Nguyen et al., 2014). To our knowledge, the effects of differing peroxy radical branching on SOA formation from nitrate radical oxidation of monoterpenes have not been investigated. The relative importance of different peroxy radical reaction channels concerning BVOCs+NO_3 chemistry in the atmosphere is not well established (Brown and Stutz, 2012). While earlier studies by Kirchner and Stockwell (1996) suggested that RO_2+NO_3 is more important in the nighttime atmosphere, a recent study by Mao et al. (2012) showed that the HO_2 mixing ratios are often on the order of 10 ppt at night. It is therefore possible that RO_2+HO_2 pathways could be important pathways in nighttime oxidation of BVOCs.

Nitrate radical chemistry is expected to produce a substantial amount of organic nitrate compounds, owing to direct addition of nitrate radical via reaction with a double bond. Organic nitrates have been observed to form a substantial portion of atmospheric aerosol in fiel studies (Brown et al., 2009; Day et al., 2010; Zaveri et al., 2010; Beaver et al., 2012; Rollins et al., 2012, 2013; Fry et al., 2013; Brown et al., 2013; Xu et al., 2015a). Organic nitrate formation has a significan impact on total NO_x lifetime, especially in NO_x-limited regions where NO_x lifetime is sensitive to the formation rates of organic nitrates (Browne and Cohen, 2012). Ambient organic nitrates can be formed through photooxidation of volatile organic compounds (VOCs) in the pres-

ence of NO_x (Chen et al., 1998; Arey et al., 2001; Yu et al., 2008) and through nitrate radical addition (Spittler et al., 2006; Perring et al., 2009; Rollins et al., 2009; Kwan et al., 2012). One removal mechanism for atmospheric organic nitrates is hydrolysis in the particle phase (e.g., Sato, 2008; Szmigielski et al., 2010; Darer et al., 2011; Hu et al., 2011; Liu et al., 2012; Rindelaub et al., 2015). Modeling studies have assumed that the majority (75 %) of the organic nitrates formed in the day are composed of tertiary nitrates based on results from the photooxidation of α-pinene and β-pinene in the presence of NO_x (Browne et al., 2013). However, the organic nitrates formed from photooxidation and nitrate radical oxidation could have different chemical structures (primary, secondary, and tertiary) and need to be investigated to better constrain the fates of organic nitrates (e.g., hydrolysis lifetime) in the atmosphere over their entire life cycle (both day and night).

The goal of this study is to determine the aerosol yields and characterize the mechanisms and chemical composition of SOA formation from the β-pinene+NO_3 system. Laboratory chamber experiments are performed in the dark under dry and humid conditions. To investigate the effects of peroxy radical fates on SOA yields and chemical composition, the experiments are designed to probe the "RO_2+NO_3" vs. "RO_2+HO_2" reaction pathways. Aerosol yields are obtained over a wide range of initial β-pinene mixing ratios. Based on the measured gas-phase and particle-phase oxidation products, mechanisms for SOA formation from β-pinene+NO_3 are proposed. Results from this study are used to evaluate the contributions of nitrate radical oxidation of monoterpenes to ambient organic aerosol measured in the southeastern United States (US), including the Southern Oxidant and Aerosol Study (SOAS) and the Southeastern Center for Air Pollution and Epidemiology (SCAPE) study.

2 Experimental

2.1 Laboratory chamber experiments

All experiments are performed in the Georgia Tech Environmental Chamber (GTEC) facility, which consists of two 12 m^3 fl xible Teflo (FEP 2 mil) chambers suspended in a 21 ft. × 12 ft. temperature-controlled enclosure. The full operational temperature range of the facility is 4–40 ± 0.5 °C. A schematic of the chamber facility is shown in Fig. 1. Each of the chambers has three Teflo manifolds with multiple sampling ports. Ports allow for the introduction of clean air, gas-phase reagents, seed aerosol, and for measurements of RH, temperature, gas-phase composition, and particle-phase composition. The chambers are surrounded by black lights (Sylvania, 24922) with output predominately in the ultraviolet region between 300 and 400 nm, with a maximum at 354 nm. The black lights are supplemented by natural sunshine fluorescen lights (Sylvania, 24477), which have wavelengths between 300 and 900 nm. The j_{NO_2} of the chamber facility is 0.28 min^{-1} when all of the black lights are turned on.

Experimental conditions are summarized in Table 1. Prior to each experiment, the chambers are cleaned by fl wing pure air (generated from AADCO, 747-14) for at least 24 h at a rate of 40 L min^{-1}, or equivalent to 0.2 chamber volumes per hour. This ensures that the ozone, NO, and NO_2 concentrations are less than 1 ppb and the particle concentration is lower than 10 cm^{-3}. Experiments are performed in the dark under either dry (RH < 2 %) or humid (RH = 50, 70 %) conditions. The air is humidifie by passing pure air through bubblers prior to introduction into the chamber. The temperature and humidity inside each Teflo chamber are measured using a hygro-thermometer (Vaisala, HMP110). Seed aerosol is generated by atomizing an ammonium sulfate solution (8 mM) or an ammonium sulfate / sulfuric acid mixture ($[(NH_4)_2SO_4]:[H_2SO_4] = 3:5$; molar ratio) into the chamber. The seed number and mass concentrations prior to typical experiments are approximately 2.0×10^4 cm^{-3} and 30 $\mu g\,m^{-3}$. The pH of the $(NH_4)_2SO_4$ seed and $(NH_4)_2SO_4$+H_2SO_4 seed at RH = 50 % is about 4.6 and 2.4, respectively, based on calculations from prior studies (Gao et al., 2004). Nucleation experiments are performed under both dry and humid (RH = 50, 70 %) conditions to determine organic aerosol density and characterize vapor wall loss effects on SOA yields. All experiments are performed at 298 K.

Experiments are designed to probe the effects of peroxy radical chemistry (RO_2+HO_2 vs. RO_2+NO_3) on SOA formation from the reaction of β-pinene with nitrate radicals. The procedure for chemical injection depends on the desired fate of the peroxy radicals in the experiments. To enhance the branching ratio of RO_2+HO_2 in the chamber experiments, formaldehyde is firs added to the chamber (Nguyen et al., 2014). Formalin solution (Sigma-Aldrich, 37 % HCHO) is injected into a glass bulb and clean air is passed over the solution until it evaporates. After this, seed aerosol, NO_2 (Matheson, 500 ppm), and ozone (generated by passing zero air through a UV radiation cell, Jelight 610, 80 ppm) are injected into the chamber. NO_2 and O_3 concentrations are chosen ($[NO_2]:[O_3] \approx 4:3$) to ensure that 99 % of the β-pinene reacts with nitrate radicals instead of ozone. The NO_2 and O_3 react to form nitrate radicals and subsequently N_2O_5 through the following reactions:

$$NO_2 + O_3 \rightarrow NO_3 + O_2, \quad \text{(R1)}$$

$$NO_3 + NO_2 \leftrightarrow N_2O_5. \quad \text{(R2)}$$

Formaldehyde then reacts with nitrate radicals to form HO_2 radicals via the following reaction:

$$HCHO + NO_3 + O_2 \rightarrow HNO_3 + CO + HO_2. \quad \text{(R3)}$$

Enough formaldehyde (3–22 ppm) is added to the chamber to ensure that the RO_2+HO_2 radical branching ratio is an order of magnitude higher than the RO_2+RO_2 and RO_2+NO_3

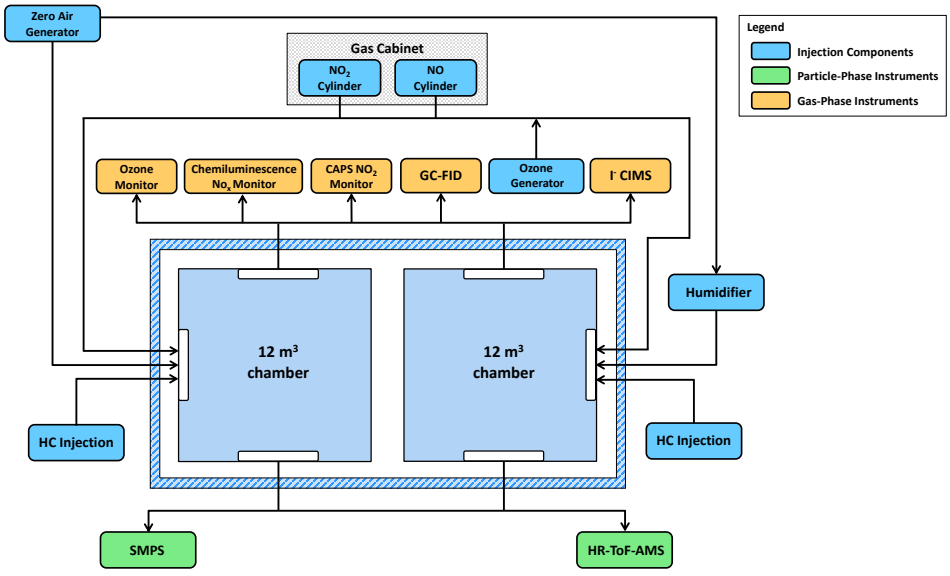

Figure 1. Schematic of the Georgia Tech Environmental Chamber (GTEC) facility.

pathways (Supplement). The chamber content is allowed to mix for ∼ 30 min, after which a desired amount of β-pinene is injected into a glass bulb, where it is introduced into the chamber by passing clean air through the glass bulb. Introduction of β-pinene into the chamber marks the beginning of the experiment. We refer to this set of experiments as "RO_2+HO_2 dominant" experiments.

For "RO_2+NO_3 dominant" experiments, seed aerosol is firs introduced into the chamber, followed by β-pinene injection. After allowing ∼ 30 min for the β-pinene concentration to stabilize, N_2O_5 is injected into the chamber. To generate N_2O_5, a mixture of NO_2 and O_3 is pre-reacted in a fl w tube (fl w rate = 1.3 L min^{-1}; residence time = 71 s) before entering the chamber. The N_2O_5 concentration is estimated by modeling the reaction of NO_2 and O_3 in the fl w tube. For this set of experiments, the introduction of N_2O_5 marks the beginning of the experiment. We aim for an initial N_2O_5 : β-pinene ratio of ∼ 6 : 1. It is noted that the ozone concentration in the chamber is sufficientl low that at least 99 % of β-pinene reacts with nitrate radicals. N_2O_5 continuously dissociates to form NO_2 and nitrate radicals during the experiment to re-establish equilibrium as the nitrate radicals react with β-pinene. The high initial N_2O_5 and nitrate radical concentrations relative to β-pinene favor the RO_2+NO_3 pathway.

For all experiments except "RO_2+HO_2 dominant" experiments conducted under humid conditions (RH = 50, 70 %), a Gas Chromatography Flame Ionization Detector (GC-FID; Agilent 6780A) measures a β-pinene concentration of zero (below detection limit) within the firs scan (scan time = 11.7 min) after the experiment begins. This suggests that β-pinene is completely consumed within 11.7 min of N_2O_5 injection for the "RO_2+NO_3 dominant" experiments and that β-pinene is fully reacted away before being detected by the GC-FID in the "RO_2+HO_2 dominant" experiments under dry conditions. The concentration of β-pinene is calculated from the mass of the hydrocarbon injected and the volume of the chamber. The chamber volume is determined to be approximately 12 m^3 by injecting a known volume of NO_2 standard (Matheson, 500 ppm) into the chamber and measuring the resulting NO_2 concentration inside the chamber.

Ozone and NO_x concentrations are monitored with an O_3 analyzer (Teledyne T400) and an ultrasensitive chemiluminescence NO_x monitor (Teledyne 200EU), respectively. Total aerosol volume and size distributions are measured with a scanning mobility particle sizer (SMPS; TSI). The SMPS consists of a differential mobility analyzer (DMA) (TSI 3040) and condensation particle counter (CPC) (TSI 3775). Bulk particle chemical composition is measured with an Aerodyne high-resolution time-of-fligh aerosol mass spectrometer (HR-ToF-AMS). The working principle and operation of the HR-ToF-AMS are described in detail elsewhere (DeCarlo et al., 2006). The HR-ToF-AMS provides quantitative measurements of organics, nitrate, sulfate, ammonium, and chloride. Elemental analysis is performed on the data to determine elemental composition (e.g., O : C, N : C ratios) of the bulk aerosol (Canagaratna et al., 2015).

A suite of gas-phase oxidation products and N_2O_5 are measured using a quadrupole chemical ionization mass spectrometer (CIMS) with I^- as the reagent ion, which has high selectivity towards reactive nitrogen species, peroxides, and carboxylic acids (Huey, 2007; McNeill et al., 2007; Zhao et al., 2012). The CIMS uses methyl iodide to produce I^- ions that ionize gas-phase products through association (Slusher et al., 2004; Zheng et al., 2011). It has been shown that I^- addition to gas-phase molecules provides a molecule–

Table 1. Experimental conditions and aerosol mass yields for all experiments.

Experiment	RH (%)	Condition	Seed	ΔHC^c (ppb)	$\Delta HC^c (\mu g m^{-3})$	$\Delta M_o^d (\mu g m^{-3})$	Mass yield (%)
1	< 2	RO_2+NO_3	AS[a]	2.5 ± 0.2	13.8 ± 1.3	5.3 ± 0.41	38.3 ± 5.5
2	< 2	RO_2+NO_3	AS	2.5 ± 0.2	13.8 ± 1.3	5.4 ± 0.15	38.7 ± 4.0
3	< 2	RO_2+NO_3	AS	7.4 ± 0.7	41.5 ± 3.9	25.3 ± 0.54	61.0 ± 6.0
4	< 2	RO_2+NO_3	AS	9.9 ± 0.9	55.4 ± 5.2	–[e]	–
5	< 2	RO_2+NO_3	AS	12.4 ± 1.2	69.2 ± 6.5	–	–
6	< 2	RO_2+NO_3	AS	12.4 ± 1.2	69.2 ± 6.5	44.9 ± 0.73	64.9 ± 6.3
7	< 2	RO_2+NO_3	AS	14.9 ± 1.4	83.0 ± 7.8	–	–
8	< 2	RO_2+NO_3	AS	17.4 ± 1.6	96.9 ± 9.1	–	–
9	< 2	RO_2+NO_3	AS	24.8 ± 2.4	138.4 ± 13.1	134.6 ± 1.51	97.2 ± 9.3
10	< 2	RO_2+NO_3	AS	24.8 ± 2.4	138.4 ± 13.1	114.7 ± 2.51	82.9 ± 8.2
11	51	RO_2+NO_3	AS	2.4 ± 0.2	13.2 ± 1.2	7.3 ± 0.57	55.4 ± 8.2
12	50	RO_2+NO_3	AS	2.4 ± 0.2	13.2 ± 1.2	6.8 ± 0.36	51.7 ± 6.3
13	49	RO_2+NO_3	AS	7.1 ± 0.7	39.6 ± 3.7	23.0 ± 0.65	57.9 ± 6.0
14	49	RO_2+NO_3	AS	9.5 ± 0.9	52.8 ± 5.0	34.2 ± 0.89	64.8 ± 6.6
15	51	RO_2+NO_3	AS	9.5 ± 0.9	52.8 ± 5.0	33.1 ± 0.56	62.5 ± 6.1
16	50	RO_2+NO_3	AS	11.9 ± 1.1	66.1 ± 6.2	43.5 ± 0.60	65.9 ± 6.4
17	50	RO_2+NO_3	AS	11.9 ± 1.1	66.1 ± 6.2	42.2 ± 0.98	63.9 ± 6.4
18	51	RO_2+NO_3	AS	14.2 ± 1.3	79.3 ± 7.5	60.7 ± 0.83	76.6 ± 7.4
19	51	RO_2+NO_3	AS	16.6 ± 1.6	92.5 ± 8.7	68.4 ± 1.26	73.9 ± 7.2
20	71	RO_2+NO_3	AS	11.9 ± 1.1	66.1 ± 6.2	50.5 ± 1.32	76.4 ± 7.8
21	70	RO_2+NO_3	AS	11.9 ± 1.1	66.1 ± 6.2	50.0 ± 0.44	75.7 ± 7.2
22	72	RO_2+NO_3	AS	23.7 ± 2.2	132.1 ± 12.5	125.5 ± 1.35	95.0 ± 9.0
23	68	RO_2+NO_3	AS	23.7 ± 2.2	132.1 ± 12.5	132.9 ± 1.33	100.6 ± 9.5
24	51	RO_2+NO_3	AS+SA[b]	7.1 ± 0.7	39.6 ± 3.7	25.5 ± 0.69	64.4 ± 6.6
25	50	RO_2+NO_3	AS+SA	11.9 ± 1.1	66.1 ± 6.2	46.4 ± 1.10	70.4 ± 6.8
26	51	RO_2+NO_3	AS+SA	16.6 ± 1.6	92.5 ± 8.7	74.4 ± 1.23	80.5 ± 7.7
27	< 3	RO_2+HO_2	AS	7.4 ± 0.7	41.5 ± 3.9	27.0 ± 0.54	64.9 ± 6.4
28	< 3	RO_2+HO_2	AS	7.4 ± 0.7	41.5 ± 3.9	22.9 ± 0.71	55.0 ± 5.8
29	< 3	RO_2+HO_2	AS	12.4 ± 1.2	69.2 ± 6.5	49.3 ± 0.97	71.2 ± 7.1
30	< 3	RO_2+HO_2	AS	12.4 ± 1.2	69.2 ± 6.5	36.1 ± 1.17	52.2 ± 5.6
31	< 2	RO_2+HO_2	AS	17.4 ± 1.6	96.9 ± 9.1	71.2 ± 2.32	73.4 ± 7.8
32	< 3	RO_2+HO_2	AS	37.3 ± 3.5	207.6 ± 19.6	216.1 ± 1.96	104.1 ± 9.9
33	49	RO_2+HO_2	AS	35.6 ± 3.4	198.2 ± 18.7	147.8 ± 1.42	74.6 ± 7.1
34	69	RO_2+HO_2	AS+SA	2.4 ± 0.2	13.2 ± 1.2	5.1 ± 0.59	38.5 ± 8.1
35	69	RO_2+HO_2	AS+SA	4.7 ± 0.4	26.4 ± 2.5	16.1 ± 1.14	61.0 ± 9.0
36	66	RO_2+HO_2	AS+SA	7.1 ± 0.7	39.6 ± 3.7	30.3 ± 0.71	76.4 ± 7.8
37	66	RO_2+HO_2	AS+SA	11.9 ± 1.1	66.1 ± 6.2	47.7 ± 1.77	72.1 ± 8.1
38	< 1	RO_2+NO_3	None	12.4 ± 1.2	69.2 ± 6.5	42.3 ± 0.46	61.1 ± 5.8
39	50	RO_2+NO_3	None	11.9 ± 1.1	66.1 ± 6.2	44.3 ± 0.34	67.0 ± 6.4
40	< 2	RO_2+HO_2	None	12.4 ± 1.2	69.2 ± 6.5	18.7 ± 0.51	27.0 ± 2.8
41	66	RO_2+HO_2	None	11.9 ± 1.1	66.1 ± 6.2	28.5 ± 0.60	43.1 ± 4.2
42	50	RO_2+HO_2	None	11.9 ± 1.1	66.1 ± 6.2	18.4 ± 0.34	27.8 ± 2.7
43	< 2	RO_2+HO_2	AS*	12.4 ± 1.2	69.2 ± 6.5	33.6 ± 0.79	48.5 ± 4.9
44	68	RO_2+HO_2	AS+SA*	11.9 ± 1.1	66.1 ± 6.2	46.6 ± 0.86	70.6 ± 7.0
45	66	RO_2+HO_2	AS+SA*	11.9 ± 1.1	66.1 ± 6.2	44.5 ± 0.87	67.3 ± 6.7

* Experiments with seed concentrations greater than the typical seed concentrations for investigating vapor wall loss effects. [a] $(NH_4)_2SO_4$ Seed. [b] $(NH_4)_2SO_4$+H_2SO_4 Seed. [c] Uncertainties in hydrocarbon concentration are calculated from an 8 % uncertainty in chamber volume and 5 % uncertainty in hydrocarbon mass. [d] Uncertainties in aerosol mass loading are calculated from 1 standard deviation of aerosol volume as measured by the SMPS. [e] "–" denotes experiments where there is no SMPS data.

iodide adduct that preserves the original species of the compounds being sampled. The gas-phase species are detected as $m/z = \mathrm{MW} + 127$. Masses with specifi m/z are selected for detection using a quadrupole mass filte . These species are then detected by an electron multiplier which amplifie incident charge through secondary electron emission to produce a measurable current that scales with gas-phase concentration. Due to unavailability of standards for the oxida-

tion products, the instrument is not calibrated for these compounds and concentrations are not reported. However, the CIMS data allow for identificatio and comparison of the abundance of specifi gas-phase oxidation products formed in different experimental conditions.

2.2 Analysis of particle-phase products

Aerosol samples are collected on Teflo filter (Pall Corp. R2PL047, 1 µm pore size and 47 mm diameter) during the SOA experiments (Experiments 9, 10, 22, 23, 32, 33 in Table 1) and for a series of blank/control experiments. These blank experiments are (1) clean chamber (no aerosol) at RH < 2 %, (2) clean chamber (no aerosol) at RH = 50 %, (3) clean chamber at RH = 50 % with only N_2O_5 injected, and (4) clean chamber at RH < 2 % with only β-pinene injected. All filter collected during the chamber experiments and controls are stored at a temperature below −20 °C before sample extraction and preparation for chromatographic analysis.

Each filte is extracted twice by sonication (Branson 3510) for 15 min in 2.50 mL acetonitrile (Fisher Optima, LC-MS grade). After combining both aliquots, each extracted sample is blown dry under a gentle stream of nitrogen (Scott-Gross, UHP), reconstituted with 1000 µL acetonitrile, and transferred to a chromatographic vial. Samples are analyzed with an Accela (Thermo Fisher Scientific ultra-high-performance liquid chromatographer (UHPLC) equipped with a 1250 quaternary delivery pump, a photodiode array detector (PDA) with a 5 cm LightPipe fl w cell, and a mass spectrometry (MS) detector (Thermo MSQ Plus). Samples are injected (50 µL) with an Accela autosampler into the reversed-phase chromatographic column (Hypersil gold C18, 50 × 2.1 mm, 1.9 µm particle size, Thermo Scientific) Excalibur software is used to control the UHPLC-PDA-MS system. Chromatographic separation at a constant fl w rate of 800 µL min^{-1} from 0 to 1 min is isocratic with 90 % (A) 0.10 mM formic acid (Fisher Optima, LC-MS grade) in ultrapure water (18.2 MΩ cm Purelab Flex, Veolia) and 10 % (B) 0.10 mM formic acid in acetonitrile. Gradient elution from 1 to 8 min reaches a 10 : 90 ratio of solvents A : B and remains isocratic from 8 to 10 min. Selected chromatograms utilize 0.4–1.0 mM acetic acid (Acros, glacial ACS, 100.0 % by assay) instead of 0.1 mM formic acid in the mobile phase. After the PDA registered the UV–visible spectra from 190 to 700 nm, the fl w is interfaced with an electrospray ionization (ESI) probe (1.9 kV needle voltage, 350 °C probe temperature, and 70 psi N_2 nebulizing gas) to the MS detector set to detect negative ions in the range of m/z 50 to 650 amu. Selected samples are analyzed under variable cone voltage (10–100 V) to register the fragmentation pattern of the peaks and gain structural information of the products. The extraction method shows an efficien 98.8 % recovery, when 98.6 µg of 4-nitrophenol (Acros, 98.0 %) are spiked onto a blank filte .

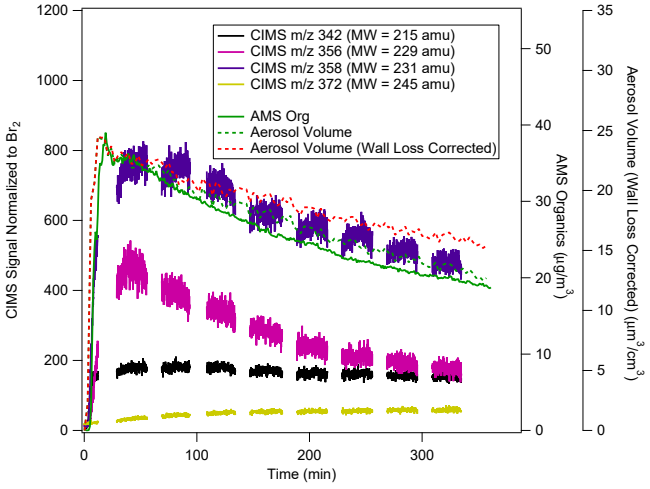

Figure 2. Time series of the gas-phase organic nitrate species measured by the CIMS and the corresponding aerosol formation measured by HR-ToF-AMS (organics mass) and SMPS (aerosol volume) (Experiment 30 in Table 1). The gas-phase species at m/z 356 decreases over the course of the experiment while the species at m/z 372 increases steadily.

3 Results

Gas-phase oxidation and aerosol growth is observed to be a rapid process in the β-pinene+NO_3 reaction. Peak aerosol growth is typically observed within 10–15 min for all reaction conditions except in humid (RH = 50, 70 %) "RO_2+HO_2 dominant" experiments, where aerosol reaches peak growth in about 30 min. Figure S1 in the Supplement shows a typical mass spectrum for the CIMS data. Specifi cally, the major gas-phase products are detected at m/z 342, 356, 358, and 372 (which correspond to MW = 215, 229, 231, 245 amu, respectively). These compounds likely correspond to organic nitrate species with molecular assignments of $C_{10}H_{17}NO_4$, $C_{10}H_{15}NO_5$, $C_{10}H_{17}NO_5$, and $C_{10}H_{15}NO_6$, respectively. Figure 2 shows the time series of these species and the aerosol growth over the course of a typical "RO_2+HO_2 dominant" experiment in dry conditions. The products at m/z 356 and 358 (MW = 229 and 231 amu) decrease over the course of the experiment. While this can be attributed to vapor phase wall loss, it is also possible that these gas-phase compounds undergo further reaction. This is further supported by the increase in the species at m/z 372 (MW = 245 amu). The proposed gas-phase oxidation mechanism and formation of compounds at m/z 372 from compounds at m/z 356 will be discussed further in Sect. 4.1.

Although all the above gas-phase species are observed under all reaction conditions, m/z 358 (MW = 231 amu) is significantl higher in the "RO_2+HO_2 dominant" experiments than in the "RO_2+NO_3 dominant" experiments (Fig. S2), which is indicative of differences in the gas-phase chemistry depending on the RO_2 fate. Under both "RO_2+HO_2 dom-

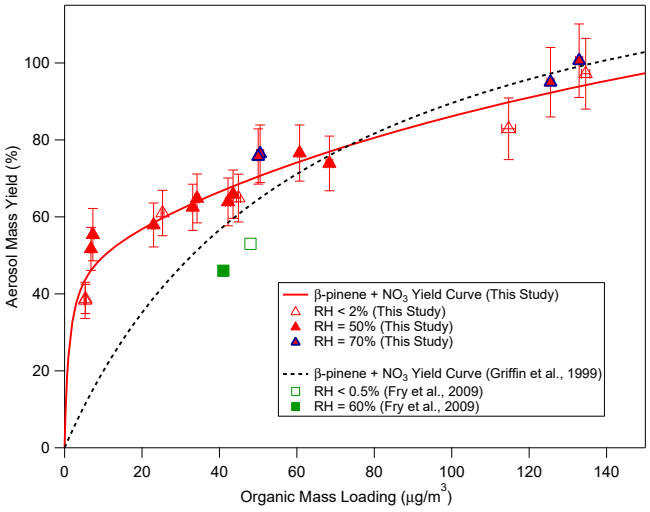

Figure 3. Aerosol mass yield as a function of organic mass loading for the β-pinene+NO_3 reaction under "RO_2+NO_3 dominant" conditions. The aerosol mass yields obtained in this study are compared to those measured in previous chamber studies by Griffi et al. (1999) and Fry et al. (2009). The aerosol mass yields obtained in this study are fitte using the two-product model proposed previously by Odum et al. (1996). The yield parameters obtained in this study and those from Griffi et al. (1999) are shown in Table 2. In order to better compare the aerosol mass yields obtained in this study to that by Griffi et al. (1999), measurements by Griffi et al. (1999) are adjusted to a temperature of 298 K and density of 1.41 g cm^{-3}. The x axis error bars represent 1 standard deviation of volume measured by SMPS at peak growth. The y axis error bars represent uncertainty in yield calculated by an 8 % uncertainty in chamber volume, 5 % uncertainty in hydrocarbon injection, and 1 standard deviation of the aerosol volume measured by SMPS at peak growth.

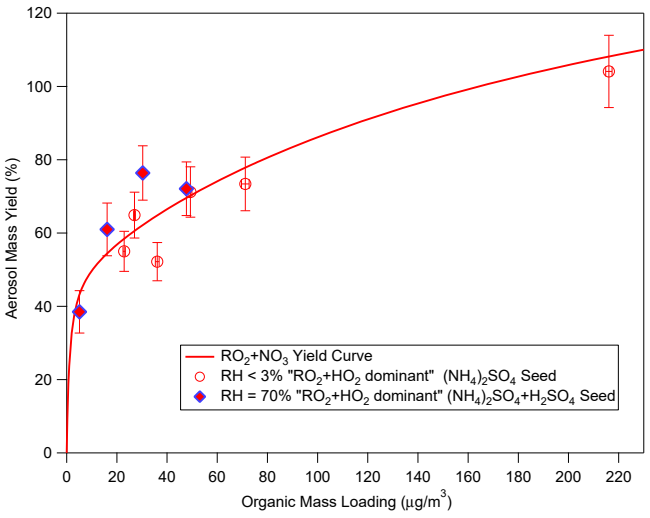

Figure 4. Aerosol mass yield as a function of organic mass loading for the β-pinene+NO_3 reaction under "RO_2+HO_2 dominant" conditions. These aerosol mass yields are compared to the yield curve (solid line) for the NO_3 + β-pinene reaction under "RO_2+NO_3 dominant" conditions. The x axis error bars represent 1 standard deviation of volume measured by SMPS at peak growth. The y axis error bars represent uncertainty in yield calculated by an 8 % uncertainty in chamber volume, 5 % uncertainty in hydrocarbon injection, and 1 standard deviation of the aerosol volume measured by SMPS at peak growth.

inant" and "RO_2+NO_3 dominant" conditions, experiments conducted under dry conditions have significantl higher N_2O_5 concentrations than humid conditions (by at least a factor of 2) as measured by CIMS. This is likely due to N_2O_5 uptake (loss) on the wet chamber surfaces and/or seed aerosol. The relative abundance of N_2O_5 under different experimental conditions is important in terms of β-pinene reaction rate and aging of aerosol, which are discussed in Sect. 4.2.2 and 4.4, respectively.

All SOA growth data are corrected for particle wall loss by applying size-dependent coefficient determined from wall loss experiments at GTEC following the methodology described in Keywood et al. (2004). The size-dependent particle wall loss rates calculated for both chambers at GTEC are shown in Fig. S3. Figures 3 and 4 show the SOA yields for "RO_2+NO_3 dominant" and "RO_2+HO_2 dominant" experiments over a wide range of aerosol mass loadings (ΔM_o = 5.1–216.1 μg m^{-3}). The SOA yields lie in the range of 27.0–104.1 % over the conditions studied. Aerosol mass yield (Y) is define as the aerosol mass concentration produced (ΔM_o) divided by the mass concentration of hydrocarbon reacted (ΔHC), $Y = \Delta M_o/\Delta\mathrm{HC}$ (Odum et al., 1996; Bowman et al., 1997; Odum et al., 1997a, b). For all experiments, aerosol mass concentration is obtained from the SMPS aerosol volume concentration (averaged over 30 min at peak growth) and the calculated aerosol density. The aerosol density is calculated from the SMPS volume distribution and the HR-ToF-AMS mass distribution in the nucleation experiments (Bahreini et al., 2005). The densities of the organic aerosol generated in nucleation experiments under dry and humid (RH = 50, 70 %) conditions are determined to be 1.41 g cm^{-3} and 1.45 g cm^{-3} for the "RO_2+NO_3 dominant" experiments and 1.54 and 1.61 g cm^{-3} for the "RO_2+HO_2 dominant" experiments.

It can be seen from Fig. 3 that the aerosol yields in the "RO_2+NO_3 dominant" experiments under dry vs. humid conditions in the presence of $(NH_4)_2SO_4$ seed are similar. The presence of the more acidic $(NH_4)_2SO_4$+H_2SO_4 seed does not appear to enhance SOA production in the "RO_2+NO_3 dominant" experiments (Fig. S4). Therefore, we fi the Odum two-product model (Odum et al., 1996, 1997a) to all of our experimental data shown in Fig. 3 to obtain a single yield curve. The SOA yield parameters are given in Table 2. Shown in Fig. 4 are the aerosol yields from "RO_2+HO_2 dominant" experiments under dry vs. humid (RH = 70 %) conditions. The SOA yield curve (solid

Table 2. Fit parameters for two-product model proposed by Odum et al. (1996).

	α_1	K_1	α_2	K_2
β-pinene+NO_3 (this study)	1.187	0.004546	0.496	0.880
Griffi et al. (1999)	1.464	0.0158		

red line) for the "RO_2+NO_3 dominant" experiments is also shown for comparison.

For comparison, SOA yields from previous β-pinene+NO_3 laboratory chamber studies (Griffi et al., 1999; Fry et al., 2009) are also shown in Fig. 3. Without adding HCHO as an additional HO_2 source, it is likely that the experiments in Griffi et al. (1999) and Fry et al. (2009) are more similar to our "RO_2+NO_3 dominant" experiments. Specificall , Fry et al. (2009) noted that the β-pinene+NO_3 reaction likely does not produce significan concentrations of HO_2 radicals and therefore has a low HO_2 / RO_2 ratio. As Griffi et al. (1999) assumed an aerosol density of 1.0 g cm^{-3}, the experimental data from Griffi et al. (1999) shown in Fig. 3 have been multiplied by the density calculated in our study for "RO_2+NO_3 dominant" experiments under dry conditions (i.e., 1.41 g cm^{-3}). The data shown in Fig. 3 from Fry et al. (2009) have also incorporated a particle density of 1.6 g cm^{-3} calculated in their study. In addition to correcting for density, the equilibrium partitioning coefficient K, from Griffi et al. (1999) has been adjusted from 306 to 298 K using an enthalpy of vaporization of 42 kJ mol^{-1} for comparison to results from our study (Chung and Seinfeld, 2002). It is noted that the SOA yields obtained in the current study are higher than those in Griffi et al. (1999) and Fry et al. (2009), particularly at lower aerosol mass loadings that are more relevant to ambient environments. These results are discussed in more detail in Sect. 4.2.

Bulk aerosol composition from the experiments is characterized by the HR-ToF-AMS. A typical high-resolution mass spectrum for aerosol formed under dry conditions where the RO_2+NO_3 pathway is dominant (Experiment 5 in Table 1) is shown in Fig. 5. A key feature of the mass spectrum is the high intensity of the nitrate ions at NO^+ and NO_2^+, which make up about 11 % of the combined organics and nitrate signals. The majority (> 90 %) of the nitrogen atoms are detected at these two ions with the remaining nitrogen-containing ions detected at higher masses as $C_xH_yO_zN$. The mass spectra for the aerosol generated in the "RO_2+HO_2 dominant" and "RO_2+NO_3 dominant" experiments are similar. One notable difference between the "RO_2+HO_2 dominant" and "RO_2+NO_3 dominant" experiments is the $NO^+ : NO_2^+$ ratio for the organic nitrates (R-ON), which ranges from 4.8 to 10.2 in all experiments. While the $NO^+ : NO_2^+$ ratio averages 6.5 for "RO_2+NO_3 dominant" experiments, it averages 8.6 for "RO_2+HO_2 dominant" experiments. Since the values of R-ON may depend on the instrument, we normalize the R-ON to the $NO^+ : NO_2^+$ ratio of ammonium nitrate (R-AN), which is expected to be a better metric (Farmer et al., 2010). In our study, multiple measurements of R-AN are obtained from the ionization efficien y (IE) calibrations and the average value is 1.8 (range of 1.2–2.7). Applying the R-AN that is measured closest in time to each chamber experiment, we calculate the average R-ON : R-AN ratio to be 3.2 for "RO_2+NO_3 dominant" experiments and 4.8 for "RO_2+HO_2 dominant" experiments.

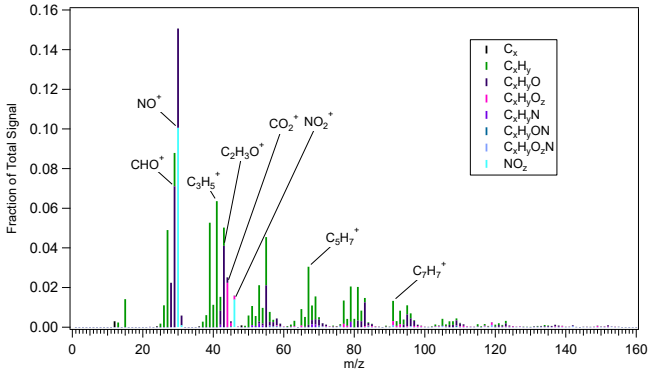

Figure 5. High-resolution aerosol mass spectrum of the SOA formed from the β-pinene+NO_3 reaction under dry, ammonium sulfate seed, and "RO_2+NO_3 dominant" conditions (Experiment 5 in Table 1). The mass spectrum is colored by the ion type to indicate the contribution of each ion type to the mass spectrum. Only ions up to m/z 160 are shown as the signals beyond m/z 160 are minimal. Ions that contribute significantl to the total signal are also labeled.

For both types of experiments, there is a negligible difference in the mass spectrum of the aerosol produced in dry or high humidity (RH = 50, 70 %) conditions. In Fig. 5, nitrate and organic ions are each assigned a different color to indicate an individual AMS HR ion family. There are a few notable ions in the aerosol mass spectrum. The signals at m/z 67 ($C_5H_7^+$) and m/z 91 ($C_7H_7^+$), while not significan in the high-resolution mass spectra of several biogenic SOA systems (Ng et al., 2008; Chhabra et al., 2010), are relatively large for β-pinene+NO_3 SOA. These ions also make up a larger fraction of the HR-ToF-AMS signal for SOA formed from the ozonolysis of β-caryophyllene (Chen et al., 2015) when compared to other biogenic SOA. Therefore, m/z 67 ($C_5H_7^+$) and m/z 91 ($C_7H_7^+$) could potentially serve as useful indicators for SOA formed from monoterpene/sesquiterpene oxidation in ambient aerosol mass spectra. However, more studies of SOA formed from the oxidation of biogenic VOCs are necessary to apportion ambient organic aerosol (OA) based on these fragments.

Figure 6 shows the time evolution of the major organic families relative to sulfate measured by the HR-ToF-AMS for a typical dry "RO_2+NO_3 dominant" experiment (Experiment 5 in Table 1). Sulfate is used to normalize the decay of the organic families because it is non-volatile and

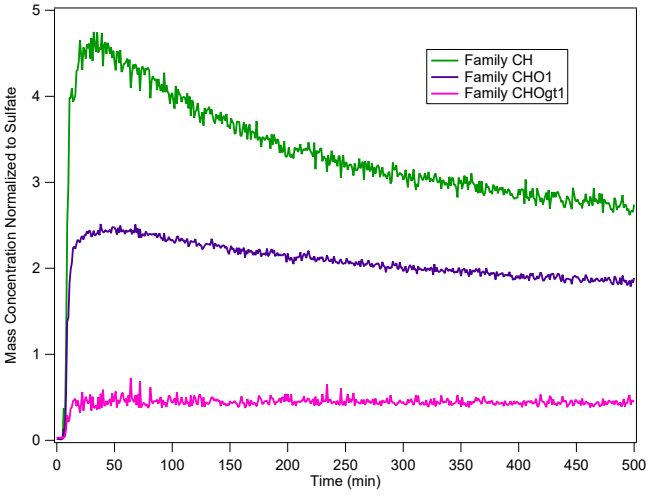

Figure 6. Time series of mass concentrations of the major organic families (normalized to the sulfate mass concentration) as measured by the HR-ToF-AMS at RH < 2 % under "RO_2+NO_3 dominant" conditions (Experiment 5 in Table 1). The least oxidized organic species (i.e., CH Family) decreases rapidly at the start of the experiment and has the largest decrease among the three major organic families.

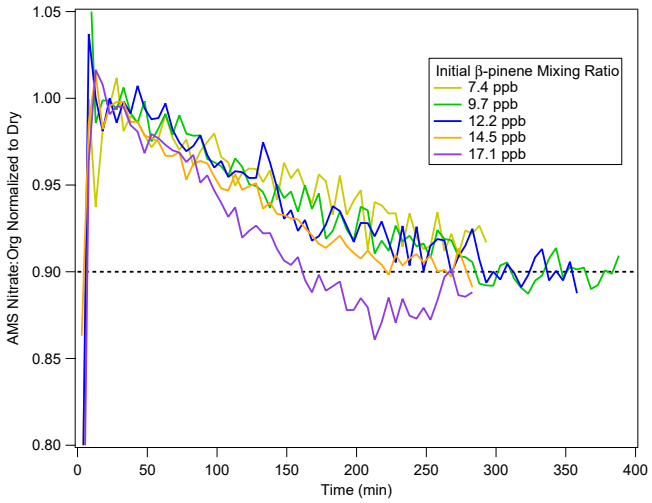

Figure 7. The AMS nitrate : org ratio of humid (RH = 50 %) experiments normalized to the corresponding dry experiments with same initial β-pinene mixing ratio, 5 min averaged, for "RO_2+NO_3 dominant" experiments. This ratio is referred to as $(\text{nitrate} : \text{org})_{\text{norm}}$ in the main text. For comparison purposes, all data are normalized to the highest $(\text{nitrate} : \text{org})_{\text{norm}}$ ratio.

any decrease in sulfate is reflect ve of particle wall loss and changes in aerosol collection efficien y (CE) in the HR-ToF-AMS (Henry and Donahue, 2012). Any change of each organic family relative to sulfate is therefore interpreted as a change in organic mass unrelated to particle wall loss or CE. Non-oxidized fragments (CH Family in green) decrease more rapidly relative to sulfate than the more oxidized fragments (CHO1 Family in purple; CHOgt1 (fragments with greater than 1 oxygen atom) Family in pink). The change in mass for each organic family is determined over a 2.5 h period following peak aerosol growth (at $t \sim 15$ min) in each "RO_2+NO_3 dominant" experiment (dry and humid). We fin that the CHOgt1 Family increases by 4 % in dry experiments and remains relatively constant in humid experiments. This is consistent with a larger extent of aerosol aging in the dry experiments and is further discussed in Sect. 4.4.

Figure 7 shows the time evolution of HR-ToF-AMS nitrate-to-organics ratio in the "RO_2+NO_3 dominant" experiments at RH = 50 % normalized by that in the corresponding dry experiments with the same initial hydrocarbon concentration. For simplicity, we refer to this ratio as $(\text{nitrate} : \text{org})_{\text{norm}}$. Normalizing the nitrate-to-organics ratio obtained from the humid experiments to the dry experiments allows for determining the extent of possible organic nitrate hydrolysis under humid conditions. Since only the relative change in the $(\text{nitrate} : \text{org})_{\text{norm}}$ ratio is important for comparison purposes, the maximum $(\text{nitrate} : \text{org})_{\text{norm}}$ measurement for each experiment is set to be unity. Nitrate mass is define here as the sum of the mass of the NO^+ and NO_2^+ ions. This does not account for the $C_xH_yO_zN$ fragments, but these fragments only account for less than 10 % (by mass) of the nitrate functional groups detected by HR-ToF-AMS. As the experiment progresses, the $(\text{nitrate} : \text{org})_{\text{norm}}$ ratio decreases and stabilizes at a value of about 0.9, indicating that there is no further decrease in the mass of nitrate relative to the mass of organics beyond this point. From our particle wall loss experiments, we establish that the particles are lost to the chamber wall with comparable rates under dry and humid conditions, suggesting that the observed decrease in the $(\text{nitrate} : \text{org})_{\text{norm}}$ ratio is not a result of differing particle wall loss in dry and humid experiments. Instead, the decrease under humid conditions is attributed to hydrolysis of organic nitrate compounds in the particle phase. This is further discussed in Sect. 4.3.2.

4 Discussion

4.1 Proposed mechanisms

Figure 8 shows the proposed scheme for the generation of species observed by CIMS and UHPLC-PDA-MS analyses from the oxidation of β-pinene with nitrate radicals. The oxidation process starts with Reaction (R1) for the sterically preferred addition of nitrate radical to the primary carbon (C_1) in the double bond of β-pinene (Wayne et al., 1991). The tertiary alkyl radical formed on C_2 can undergo (1) addition of O_2 to form a peroxy radical via Reaction (R2) (Atkinson and Arey, 2003b), (2) a 1,5-CH_3 shift indicated by Reaction (R3) (Miller, 2003) and, (3) rearrangement via Reaction (R4) (Stolle et al., 2009; Schröder et al., 2010). Reaction (R4)

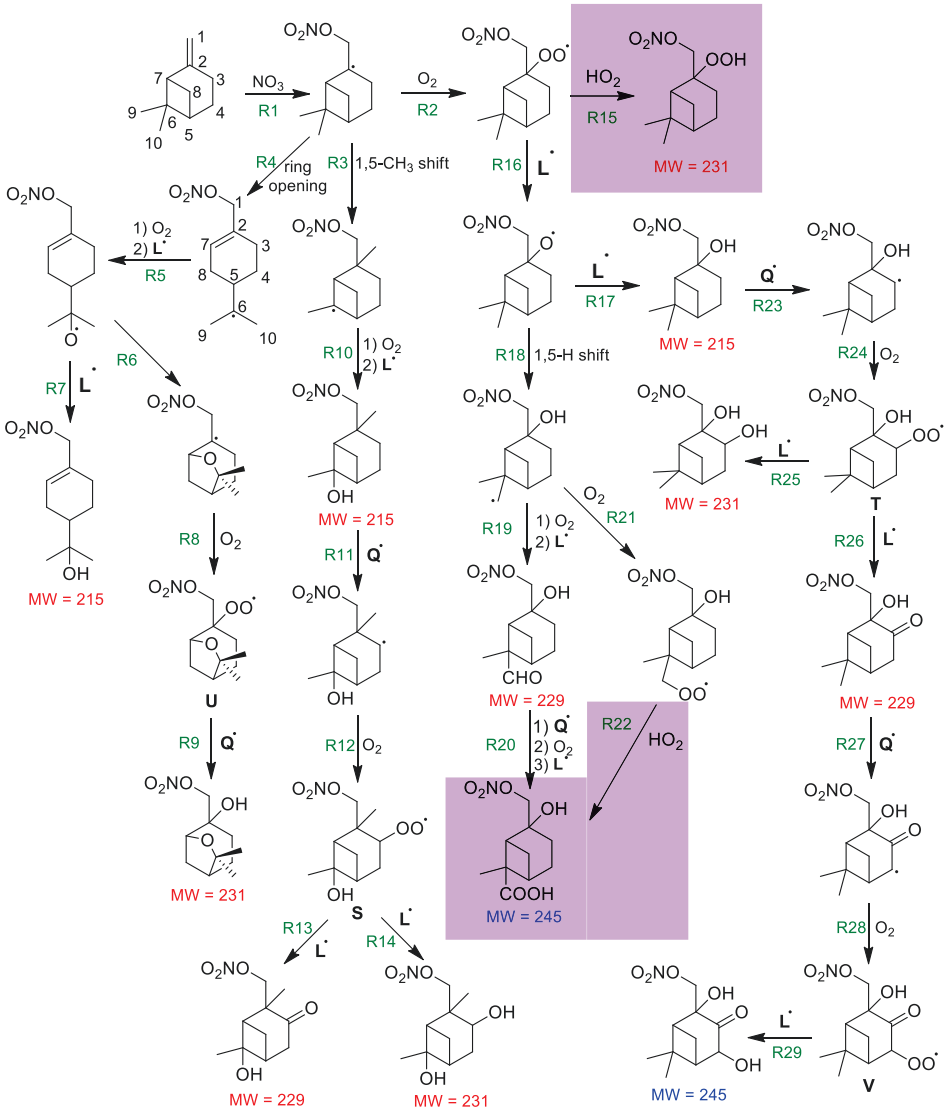

Figure 8. Generation of gas-phase species with molecular weights (MW) of 215, 229, and 231 amu detected by CIMS (red font), aerosol species with MW = 245 amu in filter analyzed by UHPLC-MS (blue font). Reaction numbers are given in green font and reaction with generic radical $\mathbf{Q}^{\bullet}$ (e.g., NO_3, RO_2) is used to symbolize any species abstracting hydrogen atoms. Reactions which can be accomplished by any of the radicals present (RO_2, HO_2, NO_3, etc.) are symbolized by reaction with generic radical $\mathbf{L}^{\bullet}$. Reactions enhanced in the RO_2+HO_2 dominant pathway are highlighted in purple.

is thought to be a favorable pathway because it relieves the ring strain from the cyclobutane while generating a tertiary alkyl radical with a new reactive double bond. In the presence of oxygen, O_2 combines with the alkyl radical to make a peroxy radical, which is then converted to an alkoxy radical via Reaction (R5) (denoted as R^5O here) (Atkinson and Arey, 2003b; Vereecken and Peeters, 2012). Reactions which can be accomplished by any of the radicals present (RO_2, HO_2, NO_3, etc.) are symbolized by reaction with generic radical $\mathbf{L}^{\bullet}$, while hydrogen abstractions are symbolized by reaction with generic radical $\mathbf{Q}^{\bullet}$ (e.g., NO_3, RO_2). R^5O can undergo intramolecular addition to the less substituted C_7 of the newly formed double bond via Reaction (R6), generating a cyclic ether alkyl radical (Vereecken and Peeters, 2004, 2012). Alternatively, R^5O can undergo hydrogen abstraction from another species via Reaction (R7) to form a hydroxynitrate of MW = 215 amu (R^7OH), a gas-phase species detected by CIMS. The cyclic ether alkyl radical generated by Reaction (R6) combines with O_2 to make peroxy radical **U** by Reaction (R8). The fate of radical **U** is to produce a cyclic ether hydroxynitrate with MW = 231 amu via Reaction (R9) (Russell, 1957; Atkinson and Arey, 2003b). A compound with the same molecular weight as this species is detected by CIMS.

The alkyl radical formed in Reaction (R1) can also undergo a 1,5-CH_3 shift as indicated by Reaction (R3), which forms a tertiary alkyl radical that then combines with O_2 by Reaction (R10). Reaction (R10) produces a hydroxynitrate ($R^{10}OH$) with MW = 215 amu, an isomer that could also correspond to the species observed by CIMS. Further functionalization of $R^{10}OH$ continues after hydrogen abstraction by Reaction (R11), which bond strength calculations predict occurs preferentially at the C_3 position (Vereecken and Peeters, 2012). The resulting secondary alkyl radical from Reaction (R11) reacts with O_2 to form peroxy radical **S** via Reaction (R12). The reaction $\mathbf{S} + \mathbf{L}^{\bullet}$ forms either a hydroxycarbonyl nitrate with MW = 229 amu by Reaction (R13), or a dihydroxynitrate with MW = 231 amu by Reaction (R14) (Russell, 1957; Atkinson and Arey, 2003b). Both are gas-phase species detected by CIMS.

The peroxy radical formed in Reaction (R2) can be converted to a hydroperoxide with MW = 231 amu (observed in CIMS) by reaction with an HO_2 radical (R15). Since Reaction (R15) is only associated with the RO_2+HO_2 channel, the signal corresponding to the species with MW = 231 amu is expected be higher in the "RO_2+HO_2 dominant" experiments. Figure S2 shows the CIMS signal at $m/z = 358$ (MW = 231 amu) normalized to Br_2 sensitivity for each type of experiment ("RO_2+NO_3 dominant" and "RO_2+HO_2 dominant"; dry and humid conditions). The higher signal in the "RO_2+HO_2 dominant" experiments supports the formation of more ROOH species in the gas phase under this reaction condition.

The peroxy radical formed from Reaction (R2) can also be converted into an alkoxy radical, $R^{16}O$, via Reaction (R16). Hydrogen abstraction by the alkoxy radical $R^{16}O$ can form a third hydroxynitrate isomer with MW = 215 amu by Reaction (R17). Alternatively, $R^{16}O$ can undergo a 1,5-H shift from a $-CH_3$ group by Reaction (R18) to form an alkyl radical at one of the terminal carbons (Carter et al., 1976; Eberhard et al., 1995; Atkinson, 1997; Dibble, 2001). The alkyl radical then reacts with O_2 to form a peroxy radical and subsequently forms an aldehyde with MW = 229 amu by the overall Reaction (R19) (Russell, 1957; Atkinson and Arey, 2003b). The aldehydic hydrogen is especially susceptible to undergoing hydrogen abstraction (Miller, 2003), followed by O_2 addition to form a peroxy acid radical, and fi nal conversion to a carboxylic acid (Russell, 1957; Atkinson and Arey, 2003b). $R^{20}COOH$ with MW = 245 amu is produced by Reaction (R20), a species registered as an anion by UHPLC-MS at m/z 244 (MW = 245 amu) (Fig. S5). CIMS data also support the pathways via Reaction (R20) (Fig. 2). The Br_2-normalized CIMS signal for species at m/z 356 (MW = 229 amu) decreases with a subsequent increase in species at m/z 372 (MW = 245 amu) in the gas phase over the course of the experiment. Due to the lower vapor pressure of carboxylic acid species compared to carbonyl species (Pankow and Asher, 2008), the majority of carboxylic acid formed from this channel is expected to partition into the particle phase. In addition to Reaction (R20), $R^{20}COOH$ can also be formed through a more direct route by addition of O_2 to the alkyl radical product and then subsequent reaction of the peroxy radical with HO_2 via the sequence of Reactions (R18) + (R21) + (R22) (Ziemann and Atkinson, 2012).

The hydroxynitrate formed by Reaction (R17) can also undergo hydrogen abstraction at the C_3 position, as indicated by Reaction (R23). (Vereecken and Peeters, 2012). Reaction (R24) shows how O_2 addition to the resulting secondary alkyl radical gives peroxy radical **T**, which can either react with $\mathbf{L}^{\bullet}$ to form a dihydroxynitrate with MW = 231 amu via Reaction (R25) or form a hydroxycarbonyl nitrate with MW = 229 amu via Reaction (R26) (Russell, 1957; Atkinson and Arey, 2003b). In the absence of hydrogen atoms in the C_3 position, hydrogen abstraction occurs from C_4 of the hydroxycarbonyl nitrate species via Reaction (R27) (Vereecken and Peeters, 2012), which then forms a peroxy radical **V** by Reaction (R28) (Atkinson and Arey, 2003b). Reaction (R29), $\mathbf{V} + \mathbf{L}^{\bullet}$, yields a dihydroxycarbonyl nitrate with MW = 245 amu (Russell, 1957; Atkinson and Arey, 2003b). This dihydroxycarbonyl nitrate is not expected to be the species appearing in the UHPLC-MS chromatogram (Fig. S5) at m/z 244 (MW = 245 amu) because it lacks a −COOH group and likely has a higher vapor pressure than the carboxylic acid species with MW = 245 amu. Instead, it is likely that the dihydroxycarbonyl nitrate is the species observed by CIMS at m/z 372 (MW = 245 amu). A third possible isomer (not shown in Fig. 8) with MW = 245 amu and containing a non-carboxylic C = O group, could be similarly formed from the product of Reaction (R13). Likewise, other isomers to those generated after Reaction (R26) can be formed from each possible structure with MW = 229 amu, providing a wide array of precursors to form heavier MW products. The confirma tion that several isomers with MW = 245 amu are present in the filte extracts is revealed from the extracted ion chromatograph (EIC), which shows closely eluting peaks at m/z 244 (MW = 245 amu) when substituting formic acid for acetic acid (Li et al., 2011) as the modifie in the mobile phase (Fig. S5).

4.2 Aerosol yields

4.2.1 SOA yields over a wide range of organic mass loadings

The SOA yields obtained from this study are shown in Figs. 3 and 4. In recent years, it has been suggested that the loss of organic vapors to the chamber wall could affect SOA yields (Matsunaga and Ziemann, 2010; Loza et al., 2010; Yeh and Ziemann, 2014; Zhang et al., 2014, 2015). Specificall , Zhang et al. (2014) demonstrated that vapor wall loss could lead to an underestimation of SOA yields by as much as a factor of 4. To evaluate the potential effect of organic vapor wall loss on SOA yields in our study, experiments without seed are carried out at different conditions (dry and humid

(RH = 50, 70 %); "RO_2+NO_3 dominant" and "RO_2+HO_2 dominant" conditions). The yields from the nucleation experiments are reported in Fig. S9 along with the yield curve obtained from seeded experiments. The similar yields for nucleation/seeded "RO_2+NO_3 dominant" experiments (dry and humid) in our study suggest that vapor wall loss has a negligible effect on aerosol yields in these experiments. It is likely that rapid reaction of β-pinene with nitrate radicals in this study mitigates the effect of organic vapor wall loss on SOA yields. Based on the rapid SOA growth (peak growth typically achieved within 10–15 min) for these experiments, it is estimated that the effective reaction rate of β-pinene in our experiments is an order of magnitude higher than the rates reported in Zhang et al. (2014). Although the aerosol mass yields for the "RO_2+HO_2 dominant" nucleation experiments are lower than the corresponding seeded experiments, further increase in the seed concentration does not have a significan effect on yield. Zhang et al. (2014) determined that if vapor phase wall loss is significan in chamber experiments, the addition of more seed particles will lead to an increase in SOA yield. Therefore, it is likely vapor phase wall loss is also negligible in our seeded "RO_2+HO_2 dominant" experiments. It is unclear at this time why nucleation experiments have lower SOA yield only for the "RO_2+HO_2 dominant" experiments. One possibility is that the chamber wall uptake of ROOH species (which is likely higher in "RO_2+HO_2 dominant" experiments as measured by CIMS; Fig. 2) is more rapid than other gas-phase species.

A comparison of aerosol yields obtained for the oxidation of β-pinene with nitrate radicals is also shown in Fig. 3. Griffi et al. (1999) performed the firs comprehensive study of SOA formation from nitrate radical oxidation of BVOCs. The aerosol yield curve reported for β-pinene+NO_3 by Griffi et al. (1999) is shown next to our yield curve in Fig. 3. The yield curve in Griffi et al. (1999) was generated from chamber experiments with $\Delta M_o > 45\,\mu g\,m^{-3}$ (range of ΔM_o = 45–660 $\mu g\,m^{-3}$) and extrapolated down to lower loadings. The yield curve generated in the current study, however, includes measurements at mass loadings $< 10\,\mu g\,m^{-3}$ and does not require any extrapolation beyond the bounds of the data to include lower, atmospherically relevant aerosol loadings. As shown in Fig. 3, while the SOA yields from this study are consistent with Griffi et al. (1999) for $\Delta M_o > 45\,\mu g\,m^{-3}$, the yields from this study are as much as a factor of 4 higher than those reported by Griffi et al. (1999) at lower mass loadings.

Instances where the measured yields at low mass loading do not match those extrapolated from higher loadings have been observed for α-pinene ozonolysis (Presto and Donahue, 2006). We attribute this result to limitations of the two-product model, which bins all compounds into only two semi-volatile products of differing vapor pressures, to cover the entire spectrum of volatilities for all chemical products. At higher mass loadings, semi-volatile and volatile compounds can condense onto the particle phase and can potentially make up the majority of the aerosol. When a two-product yield curve is fi to high mass loadings only, the parameters are likely to be biased by the semi-volatile and high volatility products. Therefore, a yield curve fi using data from only high mass loadings will not account for the low-volatility products, which might be the minority products at high organic mass loadings. The two-product fi using high mass loadings therefore cannot be used to predict yields at low mass loadings, where the SOA is mostly comprised of low-volatility products. Since the yield curve generated as part of this study spans a wide range of organic mass loadings, the fittin parameters account for both the low-volatility products and the higher volatility products.

Table 3. Coefficient for the volatility basis set proposed by Donahue et al. (2006).

	Saturation vapor pressure, C^* ($\mu g\,m^{-3}$)			
	0.1	1	10	100
β-pinene+NO_3 (this study)	0.373	0.033	0.000	0.941
Griffi et al. (1999)	0.000	0.000	0.301	1.204

Fitting yield data to the volatility basis set described in Donahue et al. (2006) illustrates how higher volatility bins (products) are favored at higher aerosol mass loadings. The fi coefficient for the volatility basis set are shown in Table 3 for the aerosol yields of β-pinene+NO_3 from this study and that of Griffi et al. (1999). It is noted that the data from Griffi et al. (1999) have been adjusted to a temperature of 298 K and density of 1.41 $g\,cm^{-3}$ for comparison to results from our study. As seen in Table 3, the stoichiometric coefficient for the fi of Griffi et al. (1999) are weighted towards higher volatility products while the coefficient fi to the data collected in this study are distributed among lower and higher volatility products.

Fry et al. (2009) conducted a pair of β-pinene+NO_3 chamber experiments under dry and humid (RH = 60 %) conditions. Their results are also shown in Fig. 3. The yields from Fry et al. (2009) are about 20 % lower than the current study. A more recent study by Fry et al. (2014) reported aerosol mass yields in the range of 33–44 % for the β-pinene+NO_3 system at an organic mass loading of $10\,\mu g\,m^{-3}$ in a continuous fl w chamber under dry conditions. This is approximately 10–30 % lower than the yield reported at a similar mass loading in this study. While various experimental conditions can contribute to the difference in aerosol mass yields, we note that the aerosol formation rate in Fry et al. (2009, 2014) is slower than this study, which is likely caused by lower oxidant concentrations in Fry et al. (2009, 2014) compared to this study. Slower reaction times could allow more time for the gas-phase species to partition onto the chamber walls and reduce the amount that partitions onto aerosol (Ng et al., 2007b; Zhang et al., 2014). Thus, organic vapor wall loss might play a role in

the lower yields observed in Fry et al. (2009, 2014). There is a substantial difference between our β-pinene+NO_3 SOA yield and that from Hallquist et al. (1999), which reported an aerosol mass yield of 10 % for a mass loading of 4 $\mu g m^{-3}$. A possible explanation for this is that the mass of β-pinene reacted was not directly measured in Hallquist et al. (1999), instead, it was assumed that the concentration of β-pinene reacted was equivalent to the concentration of N_2O_5 reacted. If there were other loss processes for N_2O_5 in the experiments conducted by Hallquist et al. (1999), the yield reported in their study could be substantially lower than the actual aerosol yield.

4.2.2 Effects of RH and acidity on SOA yields

For the "RO_2+NO_3 dominant" experiments, the yields between experiments conducted at dry conditions with ammonium sulfate seed are similar to experiments conducted under high humidity (RH = 50 % and RH = 70 %) (Fig. 3). Our results indicate that the relative humidity does not have appreciable effects on the aerosol mass yield. These results are consistent with previous humidity effects studies on photooxidation (Nguyen et al., 2011) and nitrate radical chemistry (Bonn and Moorgat, 2002; Fry et al., 2009). However, these results are inconsistent to the study performed by Spittler et al. (2006), where lower SOA yields were obtained for the α-pinene+NO_3 system under humid conditions (RH = 20 %). Spittler et al. (2006) proposed that either the presence of water vapor altered the gas-phase chemistry or that the aerosol water on seed particles prevented gas-phase partitioning. These do not seem to be the case in our study. Similar gas-phase oxidation products are detected by CIMS under both dry and humid conditions and the organics size distribution measured by HR-ToF-AMS overlaps that of the seed aerosol, indicating that the oxidation products are condensing onto the seed particles.

The presence of aerosol water can potentially affect SOA formation through hydrolysis of organic nitrates. It has been observed in previous studies that organic nitrates in aqueous filte extract can undergo hydrolysis to form alcohols and nitric acid (Sato, 2008). The change from nitrate to hydroxyl functional groups could affect gas-particle partitioning and aerosol yields if the organic nitrates and alcohols have different vapor pressures. However, previous studies have shown that hydroxyl groups lower the vapor pressure of an organic compound to the same extent as organic nitrate groups (Pankow and Asher, 2008). In this study, hydrolysis does not appear to be a major reaction pathway for β-pinene+NO_3 SOA under humid conditions. As shown in Sect. 4.4, only < 10 % of OA undergoes hydrolysis. Thus, even if there is a difference in the vapor pressures between organic nitrates and their hydrolysis products, it is unlikely that this would affect aerosol yields in our case.

Aerosol water can also enhance SOA yields by providing a medium for water-soluble species (e.g., glyoxal) to dissolve into the particulate aqueous phase (Ervens et al., 2011). Nitrate radical addition is predicted to add predominantly to a double bond instead of cleaving carbon to carbon bonds (Wayne et al., 1991) and hence fragmentation to small carbon compounds is unlikely. As shown in Fig. 8, the proposed mechanism does not involve carbon cleaving reactions which could result in small, water-soluble compounds. This is further supported by the similarities in SOA yields between dry and humid conditions. If these carbon cleaving reactions dominate and form small, water-soluble species, the yields should be much higher for the humid conditions than the dry conditions.

We fin that aerosol acidity has a negligible effect on the SOA yield for the β-pinene+NO_3 system (Fig. S4). This is opposite to some previous studies where increases in aerosol yields have been found under acidic conditions for other SOA systems (using the same seeds as in our study), such as ozonolysis of α-pinene and photooxidation of isoprene (e.g., Gao et al., 2004; Surratt et al., 2007). Acid-catalyzed particle-phase reaction such as oligomerization has been proposed for such "acid effects". Although aerosol produced by the β-pinene+NO_3 reaction can potentially undergo oligomerization as well, it appears that the aerosol products are of low enough volatility that further particle-phase reactions (if any) do not enhance SOA yields. This indicates that the "acid effect" is likely different for different SOA systems, which would depend on the parent hydrocarbon, oxidant (ozone, OH, nitrate radicals), and other reaction conditions. In general, the SOA yields for nitrate radical oxidation of BVOCs are higher than corresponding yields in ozonolysis or OH radical oxidation (e.g., Griffi et al., 1999), suggesting that no further particle-phase reaction is needed to make the oxidation products more non-volatile and the "acid effect" could be limited.

4.2.3 Effects of RO_2+ NO_3 vs. RO_2+HO_2 chemistry on SOA yields

Previous studies have shown that the fate of peroxy radicals can have a substantial effect on SOA formation (Kroll and Seinfeld, 2008; Ziemann and Atkinson, 2012). For instance, it has been shown in laboratory chamber studies that the aerosol yields can differ by a factor of 2 depending on the RO_2 fate for the isoprene+NO_3 system (Ng et al., 2008). Although studies have proposed that RO_2+NO_3 is the major nighttime RO_2 fate in the ambient environments (Kirchner and Stockwell, 1996), results from recent fiel studies suggested that HO_2 radicals are abundant at night (Mao et al., 2012). The high HO_2 radical concentration could result in the RO_2+HO_2 reaction becoming the dominant RO_2 radical fate in the nighttime atmosphere. In our study, the experimental protocols are designed to promote the "RO_2+NO_3" or "RO_2+HO_2" reaction channel. These two scenarios would be representative of nitrate radical oxidation in environments with varying levels of NO_x. To our knowledge, this is the

firs study in which the fate of peroxy radicals is considered in SOA formation from nitrate radical oxidation of monoterpenes. A simple kinetic model based on MCMv3.2 (Saunders et al., 2003) is developed to simulate the gas-phase chemistry for the β-pinene+NO_3 reaction. The simulation results suggest that in both "RO_2+NO_3 dominant" and "RO_2+HO_2 dominant" experiments, the cross-reactions of RO_2 radicals are not a significan reaction pathway (Fig. S10). Figure 4 shows that the SOA yields from the "RO_2+HO_2 dominant" experiments are similar to the "RO_2+NO_3 dominant" experiments. The similar yields under these different reaction conditions could arise from a comparable suite of reaction products between the two reaction pathways. The reaction of RO_2+NO_3 produces an RO radical (Fig. 8, Reaction R16) which can undergo decomposition or isomerization (Orlando and Tyndall, 2012; Ziemann and Atkinson, 2012). Typically, it is expected that the RO_2+HO_2 reaction will lead to the formation of peroxides (Orlando and Tyndall, 2012; Ziemann and Atkinson, 2012). However, a recent study by Hasson et al. (2012) showed that for highly substituted peroxy radicals, the RO_2+HO_2 reaction favors the formation of RO radicals. Additionally, several previous studies showed that as carbon chain length increases (C2–C4), the RO_2+HO_2 reaction becomes less likely to form the ROOH product and more likely to form the RO product (Jenkin et al., 2007; Dillon and Crowley, 2008; Hasson et al., 2012). In the case of β-pinene+NO_3, RO_2 radicals are expected to form on the tertiary carbon as the nitrate radicals tend to attack the least substituted carbon of a double bond, leading to the formation of tertiary peroxy radicals (Wayne et al., 1991) (Fig. 8). Given β-pinene is a C10 compound and forms a highly substituted peroxy radical, we hypothesize that the RO_2+HO_2 reaction pathway in our study forms RO radicals as suggested by Hasson et al. (2012), leading to a similar peroxy radical fate as in the "RO_2+NO_3 dominant" experiments. We note that the RO_2+HO_2 reaction still leads to formation of ROOH as measured by CIMS (Fig. S2). Thus, it appears that the RO_2+HO_2 channel does not exclusively produce RO radicals in our case. Nevertheless, based on the similar SOA yields in the "RO_2+NO_3 dominant" and "RO_2+HO_2 dominant" experiments, we propose that either the RO radical is the dominant product of the RO_2+HO_2 reaction pathway, or that ROOH has a similar volatility to the products formed from the RO radicals in the "RO_2+NO_3 dominant" experiments.

SOA is collected on filter for several experiments and analyzed using UHPLC in order to characterize the particle composition. Figure 9 shows the ratios of the total areas under the UV–visible chromatograms for "RO_2+HO_2 dominant" and "RO_2+NO_3 dominant" experiments, under both humid and dry conditions. Chromatograms collected at 205, 235, and 270 nm are integrated to get the total area at each wavelength and the standard deviation from two measurements. Total areas are normalized by the estimated organic mass loading on the corresponding filters The wavelengths

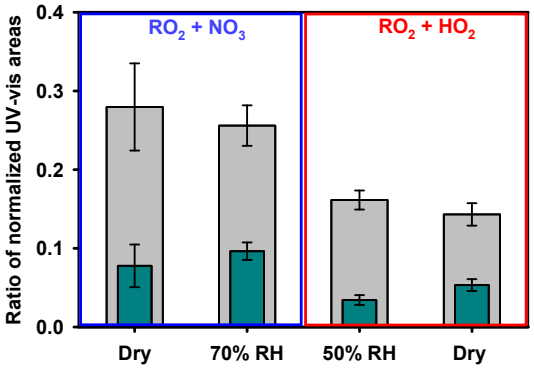

Figure 9. Ratio of the total areas integrated under UV–visible chromatograms collected at 235 nm (gray bars; ROOR and ROOH) and 270 nm (teal bars; -C=O and -ONO_2) relative to 205 nm for experiments dominated by (left-hand side panel) RO_2+NO_3 reaction and (right-hand side panel) RO_2+HO_2 reaction under both humid and dry conditions.

chosen represent a good proxy for certain functional groups that absorb in these regions. More specificall , $\lambda = 235$ nm corresponds to a region of strong absorption by ROOR and ROOH (Farmer et al., 1943; Turrà et al., 2010; Ouchi et al., 2013), while $\lambda = 270$ nm is a compromise wavelength that represents both carbonyl and alkyl nitrate functional groups (Xu et al., 1993; Pavia et al., 2008). Finally, $\lambda = 205$ nm is chosen as the normalization wavelength because practically all organic matter present in the sample absorbs in this UV region. Figure 9 shows the ratio of total areas at 235 nm and 270 nm relative to the value at 205 nm, which provides a qualitative comparison of the samples. By comparing the amounts (areas) of the 235 and 270 nm absorbing species, the effect of humidity on each branching pathway (RO_2+HO_2 or RO_2+NO_3) can be assessed. How much -ONO_2, -C = O, ROOR, and ROOH is produced under each humidity level determines the relative reactivity between the humid vs. dry conditions of each branching pathway. The relative reactivity for both reaction channels is similar within 1 standard deviation for all humidity conditions studied, indicating that each condition may have a similar product distribution. A comparison between the RO_2+ HO_2 and RO_2 + NO_3 pathways cannot be made in this manner because NO_3 concentrations are different. The seemingly smaller areas for species produced in the HO_2 panel could simply be due to a larger amount of non-nitrated organic matter being produced that absorbs at the normalization wavelength. However, one slight difference is the enhancement in the production of $C_{10}H_{15}NO_6$ (m/z 244, an RCOOH species) in the "RO_2+HO_2 dominant" experiments, which increases by 2 and 7 times under dry and humid conditions, respectively, relative to the "RO_2+NO_3 dominant" experiments. This observation indicates that in the presence of additional HO_2, the oxidation is directed toward the synthesis of $C_{10}H_{15}NO_6$ (m/z 244) more efficientl . This can be explained by an enhancement of the reaction sequence

R21 + R22 in Fig. 8, which is enhanced at high HO_2 radical concentrations.

4.3 Particulate organic nitrate formation and hydrolysis

4.3.1 Organic nitrate formation

The mass spectrum in Fig. 5 indicates the presence of a large fraction (11 %) of nitrate in the aerosol formed from the β-pinene+NO_3 reaction. Approximately 90 % of the N atoms in the spectrum are found on the NO^+ and NO_2^+ fragments. Most of the nitrate signal is assumed to be from organic species (i.e., organic nitrates) as N_2O_5 uptake to the particles is negligible and the $NO^+ : NO_2^+$ ratio is high. In humid experiments, the heterogeneous hydrolysis of N_2O_5 could lead to the formation of inorganic nitrates (e.g., HNO_3). To evaluate the contribution of inorganic nitrates to the total NO^+ and NO_2^+ ions measured by the HR-ToF-AMS, we perform two characterization experiments (RH = 50 %) in which only N_2O_5 (the maximum amount of N_2O_5 used in our aerosol experiments) and seed aerosol ($(NH_4)_2SO_4$ seed or $(NH_4)_2SO_4$+H_2SO_4 seed) are injected into the chambers. In both cases, using a relative ionization efficien y (RIE) of 1.1 for nitrate results in a nitrate growth of less than 0.1 $\mu g\,m^{-3}$ detected by the HR-ToF-AMS (Rollins et al., 2009). The uptake of N_2O_5 is even less likely in the SOA yield experiments. It has been shown that when comparing to inorganic seed only, the presence of organic matter decreased N_2O_5 uptake by 80 % (Gaston et al., 2014). Therefore, the contribution of inorganic nitrates to the total nitrate signals measured by the HR-ToF-AMS in our experiments is negligible.

It has been shown previously that the $NO^+ : NO_2^+$ ratio in the HR-ToF-AMS mass spectrum can be used to infer the presence of particle-phase organic nitrates (Farmer et al., 2010). Specificall , Farmer et al. (2010) suggested that the $NO^+ : NO_2^+$ ratio is much higher for organic nitrates (ratio = 5–15) than inorganic nitrates (ratio $\sim$ 2.7), and therefore aerosol with a high NO^+:NO_2^+ ratio likely also has a high concentration of organic nitrates. Figure 5 shows that approximately only two-thirds of the signal at m/z 30 is from NO^+, while the remaining signal is from organic CH_2O^+ fragment. At peak aerosol growth under dry and humid conditions, we determine from the high-resolution AMS data that the average R-ON value for β-pinene+NO_3 aerosol is 6.5 in "RO_2+NO_3 dominant" experiments and an average of 8.6 in "RO_2+HO_2 dominant" experiments. Previous studies (Fry et al., 2009; Bruns et al., 2010) on the β-pinene+NO_3 reaction suggested that the R-ON for β-pinene+NO_3 SOA is on the order of 10 : 1, higher that the values determined in this study. One possible explanation for the difference in R-ON between this study and previous literature is instrument bias. Different instruments may have different R-ON values. One way to circumvent this bias is to compare the R-ON : R-AN ratio. The average R-ON : R-AN for all experiments is 3.9, which is in agreement with values calculated by Fry et al. (2009) and Bruns et al. (2010) (range 3.7–4.2). Another explanation for this difference is the close proximity of the CH_2O^+ ion to the NO^+ ion in the aerosol mass spectrum, which may result in a small bias in the calculated R-ON. Specificall , if we were to include the contribution of the organic CH_2O^+ and $CH_2O_2^+$ fragments at m/z 30 and m/z 46 (in addition to contribution from NO^+ and NO_2^+) respectively, the corresponding $NO^+ : NO_2^+$ ratios would be higher, i.e., 9 : 1 for "RO_2+NO_3 dominant" experiments and 11 : 1 for "RO_2+HO_2 dominant" experiments. Therefore, when using the $NO^+ : NO_2^+$ ratio to estimate organic nitrate contribution in ambient OA, it is imperative that one excludes the organic contribution (if any) at m/z 30 when calculating the ratio.

One possible way to estimate the molar fraction of organic nitrates in the aerosol from the HR-ToF-AMS data is to use the N : C ratio (calculated by including contributions from nitrate fragments) of the aerosol formed in the experiments. Since β-pinene is a monoterpene, we assume its oxidation products have approximately 10 carbon atoms. This is a reasonable assumption based on the gas-phase oxidation products detected by CIMS (Fig. 8). The dominant reaction pathway of nitrate radicals is addition via attack of the double bond, adding one nitrate group to the primary carbon and forming a peroxy radical. With one nitrate group and 10 carbons from the β-pinene precursor, the organic nitrate products are expected to have an N : C ratio of about 1 : 10. If 100 % of the SOA formed is composed of organic nitrates, the HR-ToF-AMS data should have an N : C ratio of 0.1. The average N : C ratio for all experiments measured by the HR-ToF-AMS is approximately 0.074 for SOA formed from β-pinene+NO_3 at peak growth. Thus, as an upper bound, it is approximated that the molar fraction of organic nitrates in the aerosol is 74 %. Even if there is fragmentation, the organic nitrate fraction in the aerosol would remain fairly high. For instance, if the organic nitrate species only has nine carbons, the upper-bound molar organic nitrate fraction is approximately 67 %. If we assume the organic nitrate and non-organic nitrate species have the same molecular weight, the molar organic nitrate fraction in the aerosol is equal to the fraction of aerosol mass composed of organic nitrates. In addition to N : C, the HR-ToF-AMS nitrate : org mass ratio can also be used to estimate the particle organic nitrate fraction. The average nitrate : org mass ratio measured by the HR-ToF-AMS for all experiments is about 0.16. We assume the organic nitrate compound has an average molecular weight between 200 and 300 $g\,mol^{-1}$ based on the predicted products (Fig. 8), where 62 $g\,mol^{-1}$ is attributed to the nitrate group while the remaining mass is from the organic mass. Using both the nitrate : org mass ratio and the assumed range of molecular weights for the organic nitrate species, the fraction of aerosol mass composed of organic nitrates is estimated to be 45–68 %. We estimate that the fraction of

aerosol mass composed of organic nitrates is 60 %, based on the average value of the extremes of the two estimates. This is comparable to the fraction of aerosol mass composed of organic nitrates estimated by Fry et al. (2014) (56 %) but higher than that reported by Fry et al. (2009) (30–40 %). The different experimental conditions in our study vs. those in Fry et al. (2009) may have contributed to the difference in the fraction of aerosol mass composed of organic nitrates. For example, the ratio of NO_2 to O_3 used to make NO_3 radicals in Fry et al. (2009) is lower than this study, which may have led to differing branching ratios of β-pinene+NO_3 vs. β-pinene+O_3.

4.3.2 Hydrolysis and organic nitrate fate

As shown in Fig. 7, for experiments with the same initial hydrocarbon concentration, the AMS nitrate-to-organics ratio of the humid experiments normalized by the dry experiments stabilize at a ratio of about 0.9. The nitrate radical addition at the double bond of β-pinene can lead to the formation of either primary or tertiary nitrates. Previous studies of organic nitrate hydrolysis in bulk solutions showed that while saturated primary nitrates hydrolyze on the order of months, tertiary nitrates hydrolyze on the order of minutes (Darer et al., 2011). Primary organic nitrates with double bonds can hydrolyze on the order of minutes (Jacobs et al., 2014), but oxidation products from the β-pinene+NO_3 reaction are likely saturated compounds due to the lone double bond of β-pinene (Fig. 8). Therefore, the point at which nitrate mass stops decreasing is interpreted as when all tertiary nitrates have hydrolyzed. As the oxidation products typically contain only one nitrate group (Fig. 8), we infer that, within experimental error, approximately 90 % of the organic nitrates formed from the β-pinene+NO_3 reaction are primary nitrates. These results are consistent with finding that a nitrate radical is more likely to attack the less substituted carbon, which, in the case for β-pinene, is the terminal carbon (Wayne et al., 1991). Since the nitrate addition is the firs reaction step, any subsequent differences in peroxy radical fate (e.g., RO_2+NO_3 vs. RO_2+HO_2) will not affect the relative amount of primary vs. tertiary nitrates in our systems.

Based on the decay rate of $(\text{nitrate}:\text{org})_{\text{norm}}$, the hydrolysis lifetime of the tertiary nitrates formed in the reaction of β-pinene with nitrate radicals is calculated to be approximately 3–4.5 h. This is on the same order of magnitude as the hydrolysis lifetime (6 h) of the proposed tertiary organic nitrates formed from photooxidation of trimethyl benzene in the presence of NO_x (Liu et al., 2012). Results from our study therefore do not suggest that nitrate radical chemistry produces organic nitrates with different hydrolysis rates than what is previously known for primary or tertiary organic nitrates. Instead, this study proposes that the fraction of tertiary organic nitrates produced from nitrate radical chemistry is much lower than SOA produced from photooxidation in the presence of NO_x. While we directly demonstrate this to be true in the case of the β-pinene+NO_3 system, this can also be applied to commonly emitted terpenes, including those with internal double bonds. From the list of terpenes in Guenther et al. (2012), all unsaturated terpenes have at least one double bond with a secondary or primary carbon. For example, α-pinene contains an internal double bond connecting a tertiary carbon to a secondary carbon. The nitrate radical is more likely to attack the less substituted carbon (i.e., the secondary carbon) and form a secondary organic nitrate. As primary/secondary and tertiary organic nitrates have drastically different hydrolysis rates, it is imperative that their relative contribution be accurately represented in models when determining the fate of ambient organic nitrates. A recent study by Browne et al. (2013) modeled the hydrolysis of organic nitrates in a forested region by assuming that 75 % of atmospheric organic nitrates formed in the day are composed of tertiary organic nitrates, based on the average fraction of tertiary organic nitrates from the photooxidation of α-pinene and β-pinene in the presence of NO_x. This has implications not only on the organic nitrate fate, but also on the formation of nitric acid, a byproduct of organic nitrate hydrolysis (Sato, 2008). With this, Browne et al. (2013) predicted that hydrolysis of organic nitrates produced in the daytime could account for as much as a third to half of all nitric acid production. However, when considering organic nitrates formed both in the day and at night, the fraction of tertiary organic nitrates in ambient organic nitrates is likely lower than that used by Browne et al. (2013). This is especially true in areas where nitrate radical oxidation is the dominant source of organic nitrates (e.g., $NO_x > 75$ ppt in forested regions as noted in Browne et al., 2014). It is recommended that future modeling studies of organic nitrate fates should consider organic nitrates formed both in the day and at night in order to take into account the large contribution of primary organic nitrates (which do not hydrolyze appreciably) formed from nitrate radical oxidation of monoterpenes.

Previous studies suggested that hydrolysis of organic nitrates can be an acid-catalyzed process in both solution (Szmigielski et al., 2010) and directly in the particle phase (Rindelaub et al., 2015). However, it has been found that primary and secondary organic nitrates are stable unless the aerosol is very acidic ($\text{pH} < 0$) (Darer et al., 2011; Hu et al., 2011). We calculate the corresponding change in the $(\text{nitrate}:\text{org})_{\text{norm}}$ ratio for the experiments where $(NH_4)_2SO_4$+H_2SO_4 seed is used (data not shown in Fig. 7). We fin that for these experiments, the $(\text{nitrate}:\text{org})_{\text{norm}}$ ratio also becomes constant at around 0.9, similar to that of the $(NH_4)_2SO_4$ seed experiments. However, the experiments using $(NH_4)_2SO_4$+H_2SO_4 seed have a more rapid rate of decrease in the $(\text{nitrate}:\text{org})_{\text{norm}}$ ratio. This suggests that while hydrolysis of tertiary nitrates is accelerated under more acidic conditions, primary organic nitrates do not hydrolyze at an observable rate for the pH conditions employed in this study. As the majority of the particulate organic nitrates formed in our experiments are primary nitrates, we infer that

particle acidity may not have a significan impact on the hydrolysis of organic nitrates formed in the BVOCs+NO_3 reaction, except in the cases where the double bond on the BVOCs connects two tertiary carbons, such as terpinolene.

4.4 Aerosol aging in the dark

While the aging of SOA has been extensively investigated in multiple photooxidation studies and shown to affect aerosol mass (e.g., Donahue et al., 2012; Henry and Donahue, 2012), little is known regarding aerosol aging by nitrate radicals (Qi et al., 2012). A number of theoretical (Kerdouci et al., 2010, 2014; Rayez et al., 2014) and experimental studies (Atkinson, 1991; Wayne et al., 1991) suggested that hydrogen abstraction by nitrate radicals occurs, especially for hydrogen atoms attached to aldehyde groups. As shown in Fig. 8, the β-pinene+NO_3 reaction can lead to the formation of compounds with carbonyl groups, allowing for potential nighttime aging of SOA by nitrate radicals. We focus our aerosol aging discussion on the "RO_2+NO_3 dominant" experiments, where the oxidant (nitrate radicals) concentrations are higher.

As aerosol ages, first-generatio products either functionalize, which decreases volatility, or fragment, which can lead to an overall increase in volatility (Kroll et al., 2009). If fragmentation is the dominant pathway, a decrease in organic mass is expected as products become more volatile and repartition back to the gas phase. We use the AMS org : sulfate ratio as a proxy to examine the effect of aerosol aging on organics mass in our experiments. As wall loss of particles will lead to a decrease in organic loading, normalizing the organic loadings by sulfate allows us to examine the net change in the organics mass over the course of the experiments. The use of org : sulfate is a good proxy for aerosol aging when the organics only condense onto existing ammonium sulfate particles. A study by Loza et al. (2012) has demonstrated that in the case of rapid condensation of organic species, the timescale of condensation is less than the timescale of diffusion to existing seed particle. When in this "diffusion-limited growth" regime, the organic mass partially nucleates to form new particles. Since the nucleated particles are smaller than those particles in which ammonium sulfate acted as a seed for condensation, organics contained in these nucleated particles will be lost to the chamber walls more rapidly than the existing seed particles (Fig. S3). This could lead to an overall decrease in the org : sulfate ratio. In our study, the org : sulfate ratio decreases after SOA reaches peak growth (Fig. 6). It is possible that this decrease is caused by wall loss of organic particles formed in the diffusion-limited growth regime. It is also possible that fragmentation of aerosol components is the dominant aging pathway, resulting in a decrease in the org : sulfate ratio. Regardless, there is still evidence of increased functionalization over the course of the experiments. Rapid loss of organics due to particle wall loss or fragmentation of SOA would cause all AMS organic families to either decrease or remain constant relative to sulfate. However, Fig. 6 shows that the highly oxidized fragments (CHOgt1, fragments with greater than 1 oxygen atom) increase slightly relative to sulfate while the non-oxidized fragments (CH) are lost at nearly twice the rate as the slightly oxidized fragments (CHO1). Since non-oxidized fragments are lost more quickly than less-oxidized fragments, it is possible that further particle-phase reactions are leading to the formation of highly oxidized compounds.

For the β-pinene+NO_3 reaction, carboxylic acids can be formed from the abstraction of hydrogen from aldehydes and subsequent oxidation (Fig. 8). The observed ions at m/z 356 and m/z 372 in CIMS likely correspond to a hydroxy carbonyl nitrate and carboxylic acid, respectively. As shown in Fig. 2, m/z 356 decreases over the course of the experiment while m/z 372 increases. The possible conversion of aldehydes to carboxylic acids is also noticeable in the aerosol chemical composition. The m/z 44 (CO_2^+) fragment in the HR-ToF-AMS data likely arise from thermal decomposition of carboxylic acids (Duplissy et al., 2011) and is commonly used to infer the extent of aerosol aging (Ng et al., 2011). Although the f_{44} (fraction of CO_2^+ ion to total organics) in the typical mass spectrum of β-pinene+NO_3 SOA is low ($< 3\,\%$), there is a noticeable and continued increase in f_{44} after peak aerosol growth (Fig. 6). Specificall , during the 2.5 h following peak growth, f_{44} increases by as much as 30 % under dry conditions. Under humid conditions, the increase in f_{44} is only 6 %. These correspond to an 18 and 6 % increase in the O : C ratio (calculated without contributions from nitrate fragments) of the aerosol under dry (O : C ranging from 0.33 to 0.39 for all experiments) and humid conditions (O : C ranging from 0.33 to 0.35), respectively. The lower degree of aging in humid experiments is consistent with the observation that the CIMS N_2O_5 signals, while not quantified are clearly lower (by at least a factor of 2) in the humid "RO_2+NO_3 dominant" experiments when compared to dry experiments. This is likely due to the uptake of N_2O_5 to wet chamber and/or aerosol surfaces (Thornton et al., 2003).

It is unlikely that the observed decrease in organic species relative to sulfate and the decrease in gas phase species are due to differences in vapor phase wall loss. Matsunaga and Ziemann (2010) determined that highly oxidized gaseous organic compounds are lost to the chamber walls faster than compounds that have a lower degree of oxidation. Additionally, the gas wall partitioning coefficien for a specifi compound has also been shown to increase with decreasing vapor pressure (Yeh and Ziemann, 2014), with highly oxidized species typically having lower vapor pressures than less oxidized species (Pankow and Asher, 2008). If vapor-phase wall loss is the driving factor for the decrease of organics in this study, it would be expected that oxidized compounds would be lost to the walls more rapidly. Subsequently, these highly oxidized compounds would re-partition back to the gas phase in order to re-establish particle-gas equilibrium. The decrease in organics shown in Fig. 6, however, indicates more rapid

losses of non-oxidized fragments compared to oxidized fragments. The less oxidized species measured by CIMS (lower molecular weight) as shown in Fig. 2 also decrease more rapidly than the more oxidized species. Therefore, the change in chemical composition and decrease in vapor phase species is more likely attributable to aerosol aging than to vapor wall partitioning.

5 Relevance to ambient measurements

Results from this study provide the fundamental information to evaluate the extent to which nitrate radical oxidation of monoterpenes contributes to ambient organic aerosol. This reaction provides a direct mechanism for linking anthropogenic and biogenic emissions, and is likely substantial in the southeastern United States, where both types of emissions are high. A recent fiel campaign, SOAS, took place in Centreville, Alabama, from 01 June to 15 July 2013 to investigate the effects of anthropogenic pollution in a region with large natural emissions. Based on positive matrix factorization (PMF) analysis of the HR-ToF-AMS data obtained in SOAS, Xu et al. (2015b) identifie an OA subtype termed as less-oxidized oxygenated organic aerosol (LO-OOA), which accounted for 32 % of the total OA at Centreville. LO-OOA peaks at night and is well correlated with particle-phase organic nitrates. These suggest that LO-OOA is produced predominantly from nighttime monoterpene+NO_3 chemistry, especially from β-pinene+NO_3 as β-pinene has a high nighttime concentration (Xu et al., 2015b). Results from the current laboratory chamber study provide the relevant fundamental data for estimating the amount of aerosol produced from monoterpene+NO_3 in SOAS. The campaign-averaged loading of non-refractory PM_1 in SOAS is about 8 $\mu g m^{-3}$ and it has been determined that the aerosol is highly acidic (pH = 0.94 ± 0.59) and contains a large amount of particulate water ($5.09 \pm 3.76\,\mu g m^{-3}$) (Cerully et al., 2014; Guo et al., 2015). At night, the RH can reach up to 90 % during the SOAS measuring period (Guo et al., 2015). The current chamber study is designed to probe SOA formation from nitrate radical oxidation under atmospherically relevant loadings, under high humidity, and in the presence of seed aerosol of different acidity. The fates of peroxy radicals at night are highly uncertain, which mainly arises from the lack of constraints on the reaction rates of the peroxy radicals with other species, such as RO_2+NO_3 (Brown and Stutz, 2012). In our study, the experiments are conducted under both "RO_2+NO_3 dominant" and "RO_2+HO_2 dominant" regimes to explore the effects of peroxy radial fates on SOA formation. Using a SOA yield of 50 % (for a mass loading of 8 $\mu g m^{-3}$ obtained from the yield curve) in the presence of acidic seed at RH = 70 % obtained from "RO_2+HO_2 dominant" experiments, Xu et al. (2015b) estimated that about 50 % of nighttime OA production could be due to the reaction of monoterpenes with nitrate radicals in SOAS, a large fraction of which is from β-pinene+NO_3 reaction.

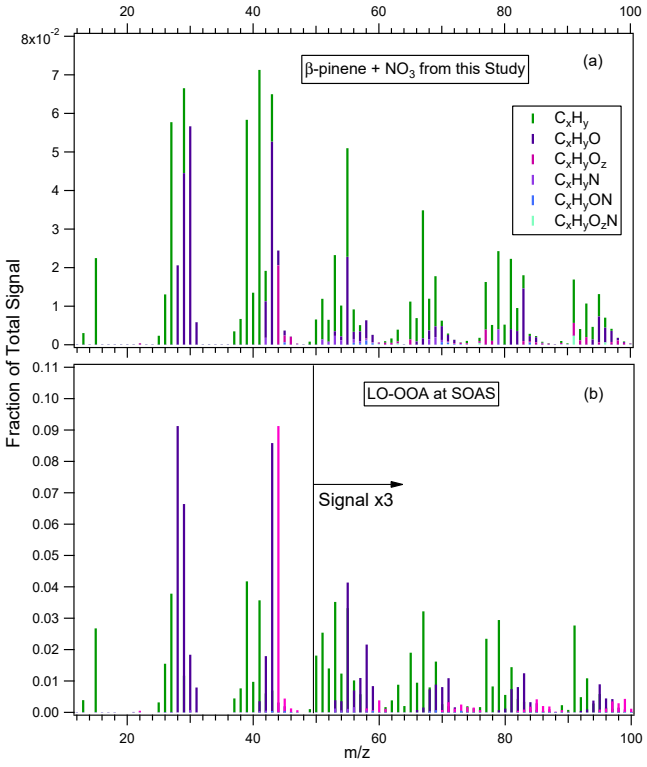

Figure 10. A comparison of mass spectra obtained from this work and the LO-OOA factor identifie from PMF analysis of the HR-ToF-AMS data from the SOAS fiel campaign. **(a)** Mass spectrum of the SOA formed from the β-pinene+NO_3 reaction at RH = 70 % under "RO_2+HO_2 dominant" conditions and $(NH_4)_2SO_4$+H_2SO_4 seed (Experiment 34 in Table 1). **(b)** Mass spectrum for the LO-OOA factor identifie from PMF analysis of the SOAS HR-ToF-AMS data (Xu et al., 2015b). The mass spectra are colored by the ion type to indicate their contribution to the mass spectra. Ions $C_5H_7^+$ (m/z 67) and $C_7H_7^+$ (m/z 91) are distinctive for the β-pinene mass spectrum (Sect. 5 of main text). To facilitate comparison, $m/z > 50$ have been multiplied by a factor of 3 in the LO-OOA spectrum.

It is noted that the LO-OOA factor is also resolved at both rural and urban sites around the greater Atlanta area in all seasons, where HR-ToF-AMS measurements were conducted as part of the SCAPE (Verma et al., 2014; Xu et al., 2015a, b). It is found that LO-OOA made up 18–36 % of the total OA in rural and urban areas, suggesting that a fairly large fraction of total OA in the southeastern United States could arise from nitrate radical oxidation of monoterpenes.

Figure 10 shows a comparison of the aerosol mass spectrum from a typical β-pinene+NO_3 experiment from this study and the LO-OOA factor obtained from SOAS data. As LO-OOA could have other sources in addition to monoterpene+NO_3, the two spectra are not in perfect agreement but they do show similar features above m/z 60. Most

noticeable of these are m/z 67 ($C_5H_7^+$) and m/z 91 ($C_7H_7^+$) with a ratio of these two ions ($C_5H_7^+$: $C_7H_7^+$) of about 2.9 (ranging from 2.5 to 3.6 in other experiments). The mass spectra for the other SOA-forming systems predicted to be of importance at SOAS, namely, α-pinene ozonolysis (Chhabra et al., 2010), isoprene photooxidation (Chhabra et al., 2010), and nitrate radical-initiated isoprene chemistry (Ng et al., 2008), do not show significan intensities at either of these two ions. Therefore, it is likely that high signals at $C_5H_7^+$ and $C_7H_7^+$ in ambient aerosol mass spectrum could be indicative of the presence of β-pinene+NO_3 reaction products. We note that the average $NO^+ : NO_2^+$ ratio for aerosol measured at SOAS is 7.1, consistent with the high $NO^+ : NO_2^+$ ratio from the SOA formed from nitrate radical oxidation of β-pinene in this study.

The gas-phase oxidation products detected by the CIMS in this study can also be used to help interpret ambient data to evaluate the possible contribution of β-pinene+NO_3 reaction. For instance, a significan amount of gas-phase organic nitrate species with MW of 215 amu and 231 amu have been observed during the Biosphere Effects of Aerosols and Photochemistry Experiment (BEARPEX) campaign in fall 2009 (Beaver et al., 2012). As these species exhibited a nighttime peak, Beaver et al. (2012) suggested that they could arise from nighttime oxidation of α-pinene or β-pinene by nitrate radicals. The proposed mechanism for β-pinene+NO_3 (Fig. 8) show multiple reaction pathways to form species with MW = 215 amu and MW = 231 amu. Therefore, the oxidation of β-pinene by nitrate radicals represents one possible pathway for the formation of the species detected by Beaver et al. (2012). As the β-pinene+NO_3 reaction has shown to be important at SOAS (Xu et al., 2015b), it is expected that the gas-phase compounds observed in this chamber study could help explain some of the species detected by the multiple CIMS deployed during the SOAS study.

6 Atmospheric implications

Although photooxidation is expected to be the major oxidation pathway for atmospheric VOCs, nitrate radical oxidation can account for as much as 20 % of global BVOC oxidation and is predicted to lead to an aerosol mass increase by as much as 45 % when compared to the modeled case where this chemistry is excluded (Pye et al., 2010). Due to high SOA yields, evaluating the mass of aerosol produced by nitrate radical-initiated chemistry is essential to estimate the total organic aerosol burden, both on regional and global scales. Currently, the aerosol yields from nitrate radical oxidation of monoterpenes in most models are assumed to be the same as those determined from β-pinene+NO_3 reactions in Griffi et al. (1999) (Pye et al., 2010). In this study, we systematically investigate SOA formation from the nitrate radical oxidation of β-pinene under various reaction conditions (dry, humid, differing radical fate) and a wide range of initial hydrocarbon concentrations that are atmospherically relevant. We determine that the SOA yields from the β-pinene+NO_3 systems are consistent with Griffi et al. (1999) for mass loadings $> 45\ \mu g\,m^{-3}$, but as much as a factor of 4 higher than those reported in Griffi et al. (1999) for lower mass loadings. The lower SOA yields reported in Griffi et al. (1999) could arise from uncertainties in extrapolating data from higher mass loadings to lower mass loadings in that study, as well as from slower reaction rates and vapor wall loss effects (Zhang et al., 2014). While it is likely that the SOA yields from the nitrate radical oxidation of various monoterpenes are different (Fry et al., 2014), updating SOA formation from β-pinene+NO_3 with the new yield parameters in future modeling studies would lead to a more accurate prediction of the amount of aerosol formed from this reaction pathway.

Currently, the fate of peroxy radicals (RO_2+HO_2 vs. RO_2+NO_3, etc.) in the nighttime atmosphere is still highly uncertain (Brown and Stutz, 2012), though recent studies showed that the HO_2 mixing ratio is often on the order of 10 ppt (Mao et al., 2012). Thus, RO_2+HO_2 could be the dominant nighttime fate of peroxy radicals. In this study, we examine the effect of RO_2 fate on aerosol yields for the β-pinene+NO_3 system. Although more ROOH species are produced through the RO_2+HO_2 channel, the SOA yields in the "RO_2+NO_3 dominant" and "RO_2+HO_2 dominant" experiments are comparable. This indicates that for this system, the overall product chemical composition and volatility distribution may not be very different for the different peroxy radical fates. This is in contrast to results from nitrate radical oxidation of smaller biogenic species, such as isoprene, which have large differences in SOA yields depending on the RO_2 fate (Ng et al., 2008). This suggests that the fates of peroxy radicals in nitrate radical experiments for larger BVOCs (such as monoterpenes and sesquiterpenes) may not be as important as it is for small compounds (such as isoprene) and in photooxidation and ozonolysis experiments (e.g., Presto et al., 2005; Kroll et al., 2006; Ng et al., 2007a; Eddingsaas et al., 2012; Xu et al., 2014); this warrants further studies.

The results from this study provide the firs insight for the specifi organic nitrate branching ratio on the β-pinene+NO_3 system. We determine that about 90 and 10 % of the organic nitrates formed from the β-pinene+NO_3 reaction are primary organic nitrates and tertiary organic nitrates, respectively. As primary and tertiary organic nitrates hydrolyze at drastically different rates, the relative contribution of primary vs. tertiary organic nitrates determined in this work would allow for improved constraints regarding the fates of organic nitrates in the atmosphere. Specificall , we fin that the primary organic nitrates do not appear to hydrolyze and the tertiary organic nitrates undergo hydrolysis with a lifetime of 3–4.5 h. Updating the branching ratio (primary vs. tertiary) with organic nitrates formed by the NO_3-initiated oxidation of BVOCs will improve model predictions of hydrolysis of organic nitrates. Hydrolysis of organic nitrates has the potential to create a long-term sink for

atmospheric nitrogen in the form of nitric acid. Organic nitrates that do not hydrolyze, however, can potentially be photolyzed or oxidized by OH radicals to release NO_x back into the atmosphere (Suarez-Bertoa et al., 2012) or lost by dry or wet deposition.

Results from this chamber study are used to evaluate the contributions from the nitrate radical oxidation of BVOCs to ambient OA in the southeastern United States, where this chemistry is expected to be substantial owing to high natural and anthropogenic emissions in the area. Factor analysis of HR-ToF-AMS data from SOAS and SCAPE fiel measurements identifie an OA subtype (LO-OOA) at these sites which is highly correlated with organic nitrates (Xu et al., 2015a, b). The β-pinene+NO_3 SOA yields obtained under reaction conditions relevant to these fiel studies are directly utilized to estimate the amount of ambient OA formed from this reaction pathway (Xu et al., 2015b). Specificall , it is estimated that 50 % of nighttime OA production occurs through the reaction of monoterpenes with nitrate radicals in SOAS (Xu et al., 2015b). Using the average R-ON : R-AN ratio obtained from this study and prior literature values, Xu et al. (2015a) estimated that organic nitrates contribute 5–12 % of total organic aerosol in the southeastern United States in summer, indicating organic nitrates are important components in ambient aerosol. Results from this study and Xu et al. (2015a, b) illustrate the substantial insights one can gain into aerosol formation chemistry and ambient aerosol source apportionment through coordinated fundamental laboratory studies and fiel measurement studies. Further, multiple gas-phase organic nitrate species are identifie in this chamber study, which could be used to help interpret ambient gas-phase composition data obtained from the large suite of gas-phase measurements in SOAS. Owing to difficultie in measuring complex atmospheric processes, laboratory studies are critical in generating fundamental data to understand and predict SOA formation regionally and globally. In this regard, it is imperative not to view laboratory studies as isolated efforts, but instead to make them essential and integrated parts of research activities in the wider atmospheric chemistry community (e.g., fiel campaigns).

The Supplement related to this article is available online at doi:10.5194/acp-15-7497-2015-supplement.

Acknowledgements. This research was funded by US Environmental Protection Agency STAR grant (Early Career) RD-83540301. L. Xu is in part supported by NSF grant 1242258 and US EPA STAR grant R834799. W. Y. Tuet is in part supported by the Health Effects Institute under research agreement no. 4943-RFA13-2/14-4. This publication's contents are solely the responsibility of the grantee and do not necessarily represent the officia views of the US EPA. Further, US EPA does not endorse the purchase of any commercial products or services mentioned in the publication. M. I. Guzman wishes to acknowledge support from NSF CAREER award (CHE-1255290). The authors would like to thank X. X. Liu, D. X. Chen, D. J. Tanner, and H. G. Huey for use and aid with their chemical ionization mass spectrometer, and to E. C. Wood for helpful discussions on the N_2O_5 injection fl w tube design.

Edited by: A. Kiendler-Scharr

References

Akagi, S. K., Yokelson, R. J., Burling, I. R., Meinardi, S., Simpson, I., Blake, D. R., McMeeking, G. R., Sullivan, A., Lee, T., Kreidenweis, S., Urbanski, S., Reardon, J., Griffith D. W. T., Johnson, T. J., and Weise, D. R.: Measurements of reactive trace gases and variable O_3 formation rates in some South Carolina biomass burning plumes, Atmos. Chem. Phys., 13, 1141–1165, doi:10.5194/acp-13-1141-2013, 2013.

Arey, J., Aschmann, S. M., Kwok, E. S. C., and Atkinson, R.: Alkyl Nitrate, Hydroxyalkyl Nitrate, and Hydroxycarbonyl Formation from the NO_x-Air Photooxidations of C5-C8 n-Alkanes, J. Phys. Chem. A, 105, 1020–1027, doi:10.1021/jp003292z, 2001.

Atkinson, R.: Kinetics and mechanisms of the gas-phase reactions of the NO_3 radical with organic-compounds, J. Phys. Chem. Ref. Data, 20, 459–507, 1991.

Atkinson, R.: Atmospheric Reactions of Alkoxy and β-Hydroxyalkoxy Radicals, Int. J. Chem. Kinet., 29, 99–111, doi:10.1002/(SICI)1097-4601(1997)29:2<99::AID-KIN3>3.0.CO;2-F, 1997.

Atkinson, R. and Arey, J.: Atmospheric degradation of volatile organic compounds, Chem. Rev., 103, 4605–4638, 2003a.

Atkinson, R. and Arey, J.: Gas-phase Tropospheric Chemistry of Biogenic Volatile Organic Compounds: A Review, Atmos. Environ., 37, 197–219, 2003b.

Bahreini, R., Keywood, M. D., Ng, N. L., Varutbangkul, V., Gao, S., Flagan, R. C., Seinfeld, J. H., Worsnop, D. R., and Jimenez, J. L.: Measurements of Secondary Organic Aerosol from Oxidation of Cycloalkenes, Terpenes, and m-Xylene Using an Aerodyne Aerosol Mass Spectrometer, Environ. Sci. Technol., 39, 5674–5688, doi:10.1021/es048061a, 2005.

Beaver, M. R., Clair, J. M. St., Paulot, F., Spencer, K. M., Crounse, J. D., LaFranchi, B. W., Min, K. E., Pusede, S. E., Wooldridge, P. J., Schade, G. W., Park, C., Cohen, R. C., and Wennberg, P. O.: Importance of biogenic precursors to the budget of organic nitrates: observations of multifunctional organic nitrates by CIMS and TD-LIF during BEARPEX 2009, Atmos. Chem. Phys., 12, 5773–5785, doi:10.5194/acp-12-5773-2012, 2012.

Berndt, T. and Boge, O.: Gas-phase reaction of NO_3 radicals with isoprene: A kinetic and mechanistic study, Int. J. Chem. Kinet., 29, 755–765, doi:10.1002/(sici)1097-4601(1997)29:10<755::aid-kin4>3.0.co;2-l, 1997a.

Berndt, T. and Boge, O.: Products and mechanism of the gas-phase reaction of NO_3 radicals with alpha-pinene, J. Chem. Soc.-Faraday Trans., 93, 3021–3027, doi:10.1039/a702364b, 1997b.

Bonn, B. and Moorgat, G. K.: New particle formation during α- and β-pinene oxidation by O_3, OH and NO_3, and the influenc of water vapour: particle size distribution studies, Atmos. Chem. Phys., 2, 183–196, doi:10.5194/acp-2-183-2002, 2002.

Bowman, F. M., Odum, J. R., Seinfeld, J. H., and Pandis, S. N.: Mathematical model for gas-particle partitioning of secondary organic aerosols, Atmos. Environ., 31, 3921–3931, doi:10.1016/s1352-2310(97)00245-8, 1997.

Brown, S. S. and Stutz, J.: Nighttime radical observations and chemistry, Chem. Soc. Rev., 41, 6405–6447, doi:10.1039/c2cs35181a, 2012.

Brown, S. S., deGouw, J. A., Warneke, C., Ryerson, T. B., Dubé, W. P., Atlas, E., Weber, R. J., Peltier, R. E., Neuman, J. A., Roberts, J. M., Swanson, A., Flocke, F., McKeen, S. A., Brioude, J., Sommariva, R., Trainer, M., Fehsenfeld, F. C., and Ravishankara, A. R.: Nocturnal isoprene oxidation over the Northeast United States in summer and its impact on reactive nitrogen partitioning and secondary organic aerosol, Atmos. Chem. Phys., 9, 3027–3042, doi:10.5194/acp-9-3027-2009, 2009.

Brown, S. S., Dubé, W. P., Bahreini, R., Middlebrook, A. M., Brock, C. A., Warneke, C., de Gouw, J. A., Washenfelder, R. A., Atlas, E., Peischl, J., Ryerson, T. B., Holloway, J. S., Schwarz, J. P., Spackman, R., Trainer, M., Parrish, D. D., Fehshenfeld, F. C., and Ravishankara, A. R.: Biogenic VOC oxidation and organic aerosol formation in an urban nocturnal boundary layer: aircraft vertical profile in Houston, TX, Atmos. Chem. Phys., 13, 11317–11337, doi:10.5194/acp-13-11317-2013, 2013.

Browne, E. C. and Cohen, R. C.: Effects of biogenic nitrate chemistry on the NO_x lifetime in remote continental regions, Atmos. Chem. Phys., 12, 11917–11932, doi:10.5194/acp-12-11917-2012, 2012.

Browne, E. C., Min, K.-E., Wooldridge, P. J., Apel, E., Blake, D. R., Brune, W. H., Cantrell, C. A., Cubison, M. J., Diskin, G. S., Jimenez, J. L., Weinheimer, A. J., Wennberg, P. O., Wisthaler, A., and Cohen, R. C.: Observations of total $RONO_2$ over the boreal forest: NO_x sinks and HNO_3 sources, Atmos. Chem. Phys., 13, 4543–4562, doi:10.5194/acp-13-4543-2013, 2013.

Browne, E. C., Wooldridge, P. J., Min, K.-E., and Cohen, R. C.: On the role of monoterpene chemistry in the remote continental boundary layer, Atmos. Chem. Phys., 14, 1225–1238, doi:10.5194/acp-14-1225-2014, 2014.

Bruns, E. A., Perraud, V., Zelenyuk, A., Ezell, M. J., Johnson, S. N., Yu, Y., Imre, D., Finlayson-Pitts, B. J., and Alexander, M. L.: Comparison of FTIR and Particle Mass Spectrometry for the Measurement of Particulate Organic Nitrates, Environ. Sci. Technol., 44, 1056–1061, doi:10.1021/es9029864, 2010.

Canagaratna, M. R., Jimenez, J. L., Kroll, J. H., Chen, Q., Kessler, S. H., Massoli, P., Hildebrandt Ruiz, L., Fortner, E., Williams, L. R., Wilson, K. R., Surratt, J. D., Donahue, N. M., Jayne, J. T., and Worsnop, D. R.: Elemental ratio measurements of organic compounds using aerosol mass spectrometry: characterization, improved calibration, and implications, Atmos. Chem. Phys., 15, 253–272, doi:10.5194/acp-15-253-2015, 2015.

Carter, W. P. L., Darnall, K. R., Lloyd, A. C., Winer, A. M., and Pitts Jr, J. N.: Evidence for Alkoxy Radical Isomerization in Photooxidations of C_4-C_6 Alkanes under Simulated Atmospheric Conditions, Chem. Phys. Lett., 42, 22–27, doi:10.1016/0009-2614(76)80543-X, 1976.

Cerully, K. M., Bougiatioti, A., Hite Jr., J. R., Guo, H., Xu, L., Ng, N. L., Weber, R., and Nenes, A.: On the link between hygroscopicity, volatility, and oxidation state of ambient and water-soluble aerosol in the Southeastern United States, Atmos. Chem. Phys. Discuss., 14, 30835–30877, doi:10.5194/acpd-14-30835-2014, 2014.

Chen, Q., Farmer, D. K., Rizzo, L. V., Pauliquevis, T., Kuwata, M., Karl, T. G., Guenther, A., Allan, J. D., Coe, H., Andreae, M. O., Pöschl, U., Jimenez, J. L., Artaxo, P., and Martin, S. T.: Submicron particle mass concentrations and sources in the Amazonian wet season (AMAZE-08), Atmos. Chem. Phys., 15, 3687–3701, doi:10.5194/acp-15-3687-2015, 2015.

Chen, X., Hulbert, D., and Shepson, P. B.: Measurement of the organic nitrate yield from OH reaction with isoprene, J. Geophys. Res.-Atmos., 103, 25563–25568, doi:10.1029/98JD01483, 1998.

Chhabra, P. S., Flagan, R. C., and Seinfeld, J. H.: Elemental analysis of chamber organic aerosol using an aerodyne high-resolution aerosol mass spectrometer, Atmos. Chem. Phys., 10, 4111–4131, doi:10.5194/acp-10-4111-2010, 2010.

Chung, S. H. and Seinfeld, J. H.: Global distribution and climate forcing of carbonaceous aerosols, J. Geophys. Res.-Atmos., 107, 4407, doi:10.1029/2001JD001397, 2002.

Darer, A. I., Cole-Filipiak, N. C., O'Connor, A. E., and Elrod, M. J.: Formation and Stability of Atmospherically Relevant Isoprene-Derived Organosulfates and Organonitrates, Environ. Sci. Technol., 45, 1895–1902, doi:10.1021/es103797z, 2011.

Day, D. A., Liu, S., Russell, L. M., and Ziemann, P. J.: Organonitrate group concentrations in submicron particles with high nitrate and organic fractions in coastal southern California, Atmos. Environ., 44, 1970–1979, doi:10.1016/j.atmosenv.2010.02.045, 2010.

DeCarlo, P. F., Kimmel, J. R., Trimborn, A., Northway, M. J., Jayne, J. T., Aiken, A. C., Gonin, M., Fuhrer, K., Horvath, T., Docherty, K. S., Worsnop, D. R., and Jimenez, J. L.: Field-deployable, high-resolution, time-of-fligh aerosol mass spectrometer, Anal. Chem., 78, 8281–8289, doi:10.1021/ac061249n, 2006.

de Gouw, J. A., Middlebrook, A. M., Warneke, C., Goldan, P. D., Kuster, W. C., Roberts, J. M., Fehsenfeld, F. C., Worsnop, D. R., Canagaratna, M. R., Pszenny, A. A. P., Keene, W. C., Marchewka, M., Bertman, S. B., and Bates, T. S.: Budget of organic carbon in a polluted atmosphere: Results from the New England Air Quality Study in 2002, J. Geophys. Res.-Atmos., 110, D16305, doi:16310.11029/12004JD005623, 2005.

Dibble, T. S.: Reactions of the alkoxy radicals formed following OH-addition to alpha-pinene and beta-pinene, C-C bond scission reactions, J. Am. Chem. Soc., 123, 4228–4234, doi:10.1021/ja003553i, 2001.

Dillon, T. J. and Crowley, J. N.: Direct detection of OH formation in the reactions of HO2 with $CH_3C(O)O_2$ and other substituted peroxy radicals, Atmos. Chem. Phys., 8, 4877–4889, doi:10.5194/acp-8-4877-2008, 2008.

Donahue, N. M., Robinson, A. L., Stanier, C. O., and Pandis, S. N.: Coupled partitioning, dilution, and chemical aging of semivolatile organics, Environ. Sci. Technol., 40, 2635–2643, doi:10.1021/es052297c, 2006.

Donahue, N. M., Henry, K. M., Mentel, T. F., Kiendler-Scharr, A., Spindler, C., Bohn, B., Brauers, T., Dorn, H. P., Fuchs, H., Tillmann, R., Wahner, A., Saathoff, H., Naumann, K.-H., Moehler, O., Leisner, T., Mueller, L., Reinnig, M.-C., Hoffmann, T., Salo, K., Hallquist, M., Frosch, M., Bilde, M., Tritscher, T., Barmet, P., Praplan, A. P., DeCarlo, P. F., Dommen, J., Prevot, A. S. H., and Baltensperger, U.: Aging of biogenic secondary organic aerosol via gas-phase OH radical reactions, Proc. Natl. Aca. Sci. USA, 109, 13503–13508, doi:10.1073/pnas.1115186109, 2012.

Duplissy, J., DeCarlo, P. F., Dommen, J., Alfarra, M. R., Metzger, A., Barmpadimos, I., Prevot, A. S. H., Weingartner, E., Tritscher, T., Gysel, M., Aiken, A. C., Jimenez, J. L., Canagaratna, M. R., Worsnop, D. R., Collins, D. R., Tomlinson, J., and Baltensperger, U.: Relating hygroscopicity and composition of organic aerosol particulate matter, Atmos. Chem. Phys., 11, 1155–1165, doi:10.5194/acp-11-1155-2011, 2011.

Eberhard, J., Muller, C., Stocker, D. W., and Kerr, J. A.: Isomerization of Alkoxy Radicals under Atmospheric Conditions, Environ. Sci. Technol., 29, 232–241, doi:10.1021/es00001a600, 1995.

Eddingsaas, N. C., Loza, C. L., Yee, L. D., Seinfeld, J. H., and Wennberg, P. O.: α-pinene photooxidation under controlled chemical conditions – Part 1: Gas-phase composition in low- and high-NO_x environments, Atmos. Chem. Phys., 12, 6489–6504, doi:10.5194/acp-12-6489-2012, 2012.

Ervens, B., Turpin, B. J., and Weber, R. J.: Secondary organic aerosol formation in cloud droplets and aqueous particles (aqSOA): a review of laboratory, fiel and model studies, Atmos. Chem. Phys., 11, 11069–11102, doi:10.5194/acp-11-11069-2011, 2011.

Farmer, D. K., Matsunaga, A., Docherty, K. S., Surratt, J. D., Seinfeld, J. H., Ziemann, P. J., and Jimenez, J. L.: Response of an aerosol mass spectrometer to organonitrates and organosulfates and implications for atmospheric chemistry, Proc. Natl. Aca. Sci. USA, 107, 6670–6675, doi:10.1073/pnas.0912340107, 2010.

Farmer, E. H., Koch, H. P., and Sutton, D. A.: The Course of Autoxidation Reactions in Polyisoprenes and Allied Compounds. Part VII. Rearrangement of Double Bonds During Autoxidation, J. Chem. Soc., 541–547, doi:10.1039/JR9430000541, 1943.

Fry, J. L., Kiendler-Scharr, A., Rollins, A. W., Wooldridge, P. J., Brown, S. S., Fuchs, H., Dubé, W., Mensah, A., dal Maso, M., Tillmann, R., Dorn, H.-P., Brauers, T., and Cohen, R. C.: Organic nitrate and secondary organic aerosol yield from NO_3 oxidation of β-pinene evaluated using a gas-phase kinetics/aerosol partitioning model, Atmos. Chem. Phys., 9, 1431–1449, doi:10.5194/acp-9-1431-2009, 2009.

Fry, J. L., Kiendler-Scharr, A., Rollins, A. W., Brauers, T., Brown, S. S., Dorn, H.-P., Dubé, W. P., Fuchs, H., Mensah, A., Rohrer, F., Tillmann, R., Wahner, A., Wooldridge, P. J., and Cohen, R. C.: SOA from limonene: role of NO_3 in its generation and degradation, Atmos. Chem. Phys., 11, 3879–3894, doi:10.5194/acp-11-3879-2011, 2011.

Fry, J. L., Draper, D. C., Zarzana, K. J., Campuzano-Jost, P., Day, D. A., Jimenez, J. L., Brown, S. S., Cohen, R. C., Kaser, L., Hansel, A., Cappellin, L., Karl, T., Hodzic Roux, A., Turnipseed, A., Cantrell, C., Lefer, B. L., and Grossberg, N.: Observations of gas- and aerosol-phase organic nitrates at BEACHON-RoMBAS 2011, Atmos. Chem. Phys., 13, 8585–8605, doi:10.5194/acp-13-8585-2013, 2013.

Fry, J. L., Draper, D. C., Barsanti, K. C., Smith, J. N., Ortega, J., Winkler, P. M., Lawler, M. J., Brown, S. S., Edwards, P. M., Cohen, R. C., and Lee, L.: Secondary Organic Aerosol Formation and Organic Nitrate Yield from NO_3 Oxidation of Biogenic Hydrocarbons, Environ. Sci. Technol., 48, 11944–11953, doi:10.1021/es502204x, 2014.

Fuentes, J., Wang, D., Bowling, D., Potosnak, M., Monson, R., Goliff, W., and Stockwell, W.: Biogenic Hydrocarbon Chemistry within and Above a Mixed Deciduous Forest, J. Atmos. Chem., 56, 165–185, doi:10.1007/s10874-006-9048-4, 2007.

Fuentes, J. D., Lerdau, M., Atkinson, R., Baldocchi, D., Bottenheim, J. W., Ciccioli, P., Lamb, B., Geron, C., Gu, L., Guenther, A., Sharkey, T. D., and Stockwell, W.: Biogenic hydrocarbons in the atmospheric boundary layer: A review, Bull. Am. Meteorol. Soc., 81, 1537–1575, doi:10.1175/1520-0477(2000)081<1537:bhitab>2.3.co;2, 2000.

Gao, S., Ng, N. L., Keywood, M., Varutbangkul, V., Bahreini, R., Nenes, A., He, J., Yoo, K. Y., Beauchamp, J. L., Hodyss, R. P., Flagan, R. C., and Seinfeld, J. H.: Particle Phase Acidity and Oligomer Formation in Secondary Organic Aerosol, Environ. Sci. Technol., 38, 6582–6589, doi:10.1021/es049125k, 2004.

Gaston, C. J., Thornton, J. A., and Ng, N. L.: Reactive uptake of N_2O_5 to internally mixed inorganic and organic particles: the role of organic carbon oxidation state and inferred organic phase separations, Atmos. Chem. Phys., 14, 5693–5707, doi:10.5194/acp-14-5693-2014, 2014.

Griffin R. J., Cocker, D. R., Flagan, R. C., and Seinfeld, J. H.: Organic aerosol formation from the oxidation of biogenic hydrocarbons, J. Geophys. Res.-Atmos., 104, 3555–3567, doi:10.1029/1998jd100049, 1999.

Guenther, A. B., Jiang, X., Heald, C. L., Sakulyanontvittaya, T., Duhl, T., Emmons, L. K., and Wang, X.: The Model of Emissions of Gases and Aerosols from Nature version 2.1 (MEGAN2.1): an extended and updated framework for modeling biogenic emissions, Geosci. Model Dev., 5, 1471–1492, doi:10.5194/gmd-5-1471-2012, 2012.

Guo, H., Xu, L., Bougiatioti, A., Cerully, K. M., Capps, S. L., Hite Jr., J. R., Carlton, A. G., Lee, S.-H., Bergin, M. H., Ng, N. L., Nenes, A., and Weber, R. J.: Fine-particle water and pH in the southeastern United States, Atmos. Chem. Phys., 15, 5211–5228, doi:10.5194/acp-15-5211-2015, 2015.

Hallquist, M., Wangberg, I., Ljungstrom, E., Barnes, I., and Becker, K. H.: Aerosol and product yields from NO_3 radical-initiated oxidation of selected monoterpenes, Environ. Sci. Technol., 33, 553–559, doi:10.1021/es980292s, 1999.

Hasson, A. S., Tyndall, G. S., Orlando, J. J., Singh, S., Hernandez, S. Q., Campbell, S., and Ibarra, Y.: Branching Ratios for the Reaction of Selected Carbonyl-Containing Peroxy Radicals with Hydroperoxy Radicals, J. Phys. Chem. A, 116, 6264–6281, doi:10.1021/jp211799c, 2012.

Hatch, L. E., Luo, W., Pankow, J. F., Yokelson, R. J., Stockwell, C. E., and Barsanti, K. C.: Identificatio and quantificatio of gaseous organic compounds emitted from biomass burning using two-dimensional gas chromatography-time-of-fligh mass spectrometry, Atmos. Chem. Phys., 15, 1865–1899, doi:10.5194/acp-15-1865-2015, 2015.

Henry, K. M. and Donahue, N. M.: Photochemical Aging of α-Pinene Secondary Organic Aerosol: Effects of OH Radical Sources and Photolysis, J. Phys. Chem. A, 116, 5932–5940, doi:10.1021/jp210288s, 2012.

Hoyle, C. R., Berntsen, T., Myhre, G., and Isaksen, I. S. A.: Secondary organic aerosol in the global aerosol – chemical transport model Oslo CTM2, Atmos. Chem. Phys., 7, 5675–5694, doi:10.5194/acp-7-5675-2007, 2007.

Hu, K. S., Darer, A. I., and Elrod, M. J.: Thermodynamics and kinetics of the hydrolysis of atmospherically relevant organonitrates and organosulfates, Atmos. Chem. Phys., 11, 8307–8320, doi:10.5194/acp-11-8307-2011, 2011.

Huey, L. G.: Measurement of trace atmospheric species by chemical ionization mass spectrometry: Speciation of reactive nitrogen and future directions, Mass Spectrom. Rev., 26, 166–184, doi:10.1002/mas.20118, 2007.

Iinuma, Y., Muller, C., Berndt, T., Boge, O., Claeys, M., and Herrmann, H.: Evidence for the existence of organosulfates from beta-pinene ozonolysis in ambient secondary organic aerosol, Environ. Sci. Technol., 41, 6678–6683, doi:10.1021/es070938t, 2007.

Jacobs, M. I., Burke, W. J., and Elrod, M. J.: Kinetics of the reactions of isoprene-derived hydroxynitrates: gas phase epoxide formation and solution phase hydrolysis, Atmos. Chem. Phys., 14, 8933–8946, doi:10.5194/acp-14-8933-2014, 2014.

Jaoui, M., Kleindienst, T. E., Docherty, K. S., Lewandowski, M., and Offenberg, J. H.: Secondary organic aerosol formation from the oxidation of a series of sesquiterpenes: alpha-cedrene, beta-caryophyllene, alpha-humulene and alpha-farnesene with O-3, OH and NO_3 radicals, Environ. Chem., 10, 178–193, doi:10.1071/en13025, 2013.

Jenkin, M. E., Hurley, M. D., and Wallington, T. J.: Investigation of the radical product channel of the $CH_3C(O)O_2 + HO_2$ reaction in the gas phase, Phys. Chem. Chem. Phys., 9, 3149–3162, doi:10.1039/B702757E, 2007.

Kanakidou, M., Seinfeld, J. H., Pandis, S. N., Barnes, I., Dentener, F. J., Facchini, M. C., Van Dingenen, R., Ervens, B., Nenes, A., Nielsen, C. J., Swietlicki, E., Putaud, J. P., Balkanski, Y., Fuzzi, S., Horth, J., Moortgat, G. K., Winterhalter, R., Myhre, C. E. L., Tsigaridis, K., Vignati, E., Stephanou, E. G., and Wilson, J.: Organic aerosol and global climate modelling: a review, Atmos. Chem. Phys., 5, 1053–1123, doi:10.5194/acp-5-1053-2005, 2005.

Kerdouci, J., Picquet-Varrault, B., and Doussin, J. F.: Prediction of Rate Constants for Gas-Phase Reactions of Nitrate Radical with Organic Compounds: A New Structure-Activity Relationship, Chem. Phys. Chem., 11, 3909–3920, doi:10.1002/cphc.201000673, 2010.

Kerdouci, J., Picquet-Varrault, B., and Doussin, J. F.: Structure-activity relationship for the gas-phase reactions of NO_3 radical with organic compounds: Update and extension to aldehydes, Atmos. Environ., 84, 363–372, doi:10.1016/j.atmosenv.2013.11.024, 2014.

Keywood, M. D., Varutbangkul, V., Bahreini, R., Flagan, R. C., and Seinfeld, J. H.: Secondary organic aerosol formation from the ozonolysis of cycloalkenes and related compounds, Environ. Sci. Technol., 38, 4157–4164, doi:10.1021/es035363o, 2004.

Kirchner, F. and Stockwell, W. R.: Effect of peroxy radical reactions on the predicted concentrations of ozone, nitrogenous compounds, and radicals, J. Geophys. Res.-Atmos., 101, 21007–21022, doi:10.1029/96JD01519, 1996.

Kroll, J. H. and Seinfeld, J. H.: Chemistry of secondary organic aerosol: Formation and evolution of low-volatility organics in the atmosphere, Atmos. Environ., 42, 3593–3624, doi:10.1016/j.atmosenv.2008.01.003, 2008.

Kroll, J. H., Ng, N. L., Murphy, S. M., Flagan, R. C., and Seinfeld, J. H.: Secondary Organic Aerosol Formation from Isoprene Photooxidation, Environ. Sci. Technol., 40, 1869–1877, doi:10.1021/es0524301, 2006.

Kroll, J. H., Smith, J. D., Che, D. L., Kessler, S. H., Worsnop, D. R., and Wilson, K. R.: Measurement of fragmentation and functionalization pathways in the heterogeneous oxidation of oxidized organic aerosol, Phys. Chem. Chem. Phys., 11, 8005–8014, doi:10.1039/b905289e, 2009.

Kwan, A. J., Chan, A. W. H., Ng, N. L., Kjaergaard, H. G., Seinfeld, J. H., and Wennberg, P. O.: Peroxy radical chemistry and OH radical production during the NO_3-initiated oxidation of isoprene, Atmos. Chem. Phys., 12, 7499–7515, doi:10.5194/acp-12-7499-2012, 2012.

Lewis, C. W., Klouda, G. A., and Ellenson, W. D.: Radiocarbon measurement of the biogenic contribution to summertime PM-2.5 ambient aerosol in Nashville, TN, Atmos. Environ., 38, 6053–6061, doi:10.1016/j.atmosenv.2004.06.011, 2004.

Li, Y. J., Chen, Q., Guzman, M. I., Chan, C. K., and Martin, S. T.: Second-generation products contribute substantially to the particle-phase organic material produced by β-caryophyllene ozonolysis, Atmos. Chem. Phys., 11, 121–132, doi:10.5194/acp-11-121-2011, 2011.

Liu, S., Shilling, J. E., Song, C., Hiranuma, N., Zaveri, R. A., and Russell, L. M.: Hydrolysis of Organonitrate Functional Groups in Aerosol Particles, Aerosol Sci. Technol., 46, 1359–1369, doi:10.1080/02786826.2012.716175, 2012.

Loza, C. L., Chan, A. W. H., Galloway, M. M., Keutsch, F. N., Flagan, R. C., and Seinfeld, J. H.: Characterization of Vapor Wall Loss in Laboratory Chambers, Environ. Sci. Technol., 44, 5074–5078, doi:10.1021/es100727v, 2010.

Loza, C. L., Chhabra, P. S., Yee, L. D., Craven, J. S., Flagan, R. C., and Seinfeld, J. H.: Chemical aging of *m*-xylene secondary organic aerosol: laboratory chamber study, Atmos. Chem. Phys., 12, 151–167, doi:10.5194/acp-12-151-2012, 2012.

Mao, J., Ren, X., Zhang, L., Van Duin, D. M., Cohen, R. C., Park, J.-H., Goldstein, A. H., Paulot, F., Beaver, M. R., Crounse, J. D., Wennberg, P. O., DiGangi, J. P., Henry, S. B., Keutsch, F. N., Park, C., Schade, G. W., Wolfe, G. M., Thornton, J. A., and Brune, W. H.: Insights into hydroxyl measurements and atmospheric oxidation in a California forest, Atmos. Chem. Phys., 12, 8009–8020, doi:10.5194/acp-12-8009-2012, 2012.

Marley, N. A., Gaffney, J. S., Tackett, M., Sturchio, N. C., Heraty, L., Martinez, N., Hardy, K. D., Marchany-Rivera, A., Guilderson, T., MacMillan, A., and Steelman, K.: The impact of biogenic carbon sources on aerosol absorption in Mexico City, Atmos. Chem. Phys., 9, 1537–1549, doi:10.5194/acp-9-1537-2009, 2009.

Matsunaga, A. and Ziemann, P. J.: Yields of beta-hydroxynitrates, dihydroxynitrates, and trihydroxynitrates formed from OH radical-initiated reactions of 2-methyl-1-alkenes, Proc. Natl. Aca. Sci. USA, 107, 6664–6669, doi:10.1073/pnas.0910585107, 2010.

McLaren, R., Salmon, R. A., Liggio, J., Hayden, K. L., Anlauf, K. G., and Leaitch, W. R.: Nighttime chemistry at a rural site in the Lower Fraser Valley, Atmos. Environ., 38, 5837–5848, doi:10.1016/j.atmosenv.2004.03.074, 2004.

McNeill, V. F., Wolfe, G. M., and Thornton, J. A.: The Oxidation of Oleate in Submicron Aqueous Salt Aerosols:? Evidence of a Surface Process, J. Phys. Chem. A, 111, 1073–1083, doi:10.1021/jp066233f, 2007.

Miller, B.: Advanced Organic Chemistry: Reactions and Mechanisms, 2nd Edn., Pearson/Prentice Hall, Lebanon, IN, 2003.

Ng, N. L., Chhabra, P. S., Chan, A. W. H., Surratt, J. D., Kroll, J. H., Kwan, A. J., McCabe, D. C., Wennberg, P. O., Sorooshian, A., Murphy, S. M., Dalleska, N. F., Flagan, R. C., and Seinfeld,

J. H.: Effect of NOx level on secondary organic aerosol (SOA) formation from the photooxidation of terpenes, Atmos. Chem. Phys., 7, 5159–5174, doi:10.5194/acp-7-5159-2007, 2007a.

Ng, N. L., Kroll, J. H., Chan, A. W. H., Chhabra, P. S., Flagan, R. C., and Seinfeld, J. H.: Secondary organic aerosol formation from *m*-xylene, toluene, and benzene, Atmos. Chem. Phys., 7, 3909–3922, doi:10.5194/acp-7-3909-2007, 2007b.

Ng, N. L., Kwan, A. J., Surratt, J. D., Chan, A. W. H., Chhabra, P. S., Sorooshian, A., Pye, H. O. T., Crounse, J. D., Wennberg, P. O., Flagan, R. C., and Seinfeld, J. H.: Secondary organic aerosol (SOA) formation from reaction of isoprene with nitrate radicals (NO3), Atmos. Chem. Phys., 8, 4117–4140, doi:10.5194/acp-8-4117-2008, 2008.

Ng, N. L., Canagaratna, M. R., Jimenez, J. L., Chhabra, P. S., Seinfeld, J. H., and Worsnop, D. R.: Changes in organic aerosol composition with aging inferred from aerosol mass spectra, Atmos. Chem. Phys., 11, 6465–6474, doi:10.5194/acp-11-6465-2011, 2011.

Nguyen, T. B., Roach, P. J., Laskin, J., Laskin, A., and Nizkorodov, S. A.: Effect of humidity on the composition of isoprene photooxidation secondary organic aerosol, Atmos. Chem. Phys., 11, 6931–6944, doi:10.5194/acp-11-6931-2011, 2011.

Nguyen, T. B., Crounse, J. D., Schwantes, R. H., Teng, A. P., Bates, K. H., Zhang, X., St. Clair, J. M., Brune, W. H., Tyndall, G. S., Keutsch, F. N., Seinfeld, J. H., and Wennberg, P. O.: Overview of the Focused Isoprene eXperiment at the California Institute of Technology (FIXCIT): mechanistic chamber studies on the oxidation of biogenic compounds, Atmos. Chem. Phys., 14, 13531–13549, doi:10.5194/acp-14-13531-2014, 2014.

Odum, J. R., Hoffmann, T., Bowman, F., Collins, D., Flagan, R. C., and Seinfeld, J. H.: Gas/Particle Partitioning and Secondary Organic Aerosol Yields, Environ. Sci. Technol., 30, 2580–2585, doi:10.1021/es950943+, 1996.

Odum, J. R., Jungkamp, T. P. W., Griffin R. J., Forstner, H. J. L., Flagan, R. C., and Seinfeld, J. H.: Aromatics, reformulated gasoline, and atmospheric organic aerosol formation, Environ. Sci. Technol., 31, 1890–1897, doi:10.1021/es960535l, 1997a.

Odum, J. R., Jungkamp, T. P. W., Griffin R. J., Flagan, R. C., and Seinfeld, J. H.: The atmospheric aerosol-forming potential of whole gasoline vapor, Science, 276, 96–99, doi:10.1126/science.276.5309.96, 1997b.

Orlando, J. J. and Tyndall, G. S.: Laboratory studies of organic peroxy radical chemistry: an overview with emphasis on recent issues of atmospheric significance Chem. Soc. Rev., 41, 6294–6317, doi:10.1039/C2CS35166H, 2012.

Ouchi, A., Liu, C., Kaneda, M., and Hyugano, T.: Photochemical C–C Bond Formation between Alcohols and Olefin by an Environmentally Benign Radical Reaction, Eur. J. Org. Chem., 2013, 3807–3816, doi:10.1002/ejoc.201300115, 2013.

Pankow, J. F. and Asher, W. E.: SIMPOL.1: a simple group contribution method for predicting vapor pressures and enthalpies of vaporization of multifunctional organic compounds, Atmos. Chem. Phys., 8, 2773–2796, doi:10.5194/acp-8-2773-2008, 2008.

Pavia, D., Lampman, G., Kriz, G., and Vyvyan, J.: Introduction to spectroscopy, Cengage Learning, 2008.

Perraud, V., Bruns, E. A., Ezell, M. J., Johnson, S. N., Greaves, J., and Finlayson-Pitts, B. J.: Identificatio of Organic Nitrates in the NO_3 Radical Initiated Oxidation of α-Pinene by Atmospheric Pressure Chemical Ionization Mass Spectrometry, Environ. Sci. Technol., 44, 5887–5893, doi:10.1021/es1005658, 2010.

Perring, A. E., Wisthaler, A., Graus, M., Wooldridge, P. J., Lockwood, A. L., Mielke, L. H., Shepson, P. B., Hansel, A., and Cohen, R. C.: A product study of the isoprene+NO_3 reaction, Atmos. Chem. Phys., 9, 4945–4956, doi:10.5194/acp-9-4945-2009, 2009.

Presto, A. A. and Donahue, N. M.: Investigation of alpha-pinene plus ozone secondary organic aerosol formation at low total aerosol mass, Environ. Sci. Technol., 40, 3536–3543, doi:10.1021/es052203z, 2006.

Presto, A. A., Huff Hartz, K. E., and Donahue, N. M.: Secondary Organic Aerosol Production from Terpene Ozonolysis. 2. Effect of NO_x Concentration, Environ. Sci. Technol., 39, 7046–7054, doi:10.1021/es050400s, 2005.

Pye, H. O. T., Chan, A. W. H., Barkley, M. P., and Seinfeld, J. H.: Global modeling of organic aerosol: the importance of reactive nitrogen (NO_x and NO_3), Atmos. Chem. Phys., 10, 11261–11276, doi:10.5194/acp-10-11261-2010, 2010.

Qi, L., Nakao, S., and Cocker III, D. R.: Aging of secondary organic aerosol from alpha-pinene ozonolysis: Roles of hydroxyl and nitrate radicals, J. Air Waste Manage. Assoc., 62, 1359–1369, doi:10.1080/10962247.2012.712082, 2012.

Rastogi, N., Zhang, X. L., Edgerton, E. S., Ingall, E., and Weber, R. J.: Filterable water-soluble organic nitrogen in fin particles over the southeastern USA during summer, Atmos. Environ., 45, 6040–6047, doi:10.1016/j.atmosenv.2011.07.045, 2011.

Rayez, M.-T., Rayez, J.-C., Kerdouci, J., and Picquet-Varrault, B.: Theoretical Study of the Gas-Phase Reactions of NO_3 Radical with a Series of trans-2-Unsaturated Aldehydes: From Acrolein to trans-2-Octenal, J. Phys. Chem. A, 118, 5149–5155, doi:10.1021/jp503619d, 2014.

Rindelaub, J. D., McAvey, K. M., and Shepson, P. B.: The photochemical production of organic nitrates from α-pinene and loss via acid-dependent particle phase hydrolysis, Atmos. Environ., 100, 193–201, doi:10.1016/j.atmosenv.2014.11.010, 2015.

Rollins, A. W., Kiendler-Scharr, A., Fry, J. L., Brauers, T., Brown, S. S., Dorn, H.-P., Dubé, W. P., Fuchs, H., Mensah, A., Mentel, T. F., Rohrer, F., Tillmann, R., Wegener, R., Wooldridge, P. J., and Cohen, R. C.: Isoprene oxidation by nitrate radical: alkyl nitrate and secondary organic aerosol yields, Atmos. Chem. Phys., 9, 6685–6703, doi:10.5194/acp-9-6685-2009, 2009.

Rollins, A. W., Browne, E. C., Min, K. E., Pusede, S. E., Wooldridge, P. J., Gentner, D. R., Goldstein, A. H., Liu, S., Day, D. A., Russell, L. M., and Cohen, R. C.: Evidence for NO_x Control over Nighttime SOA Formation, Science, 337, 1210–1212, doi:10.1126/science.1221520, 2012.

Rollins, A. W., Pusede, S., Wooldridge, P., Min, K. E., Gentner, D. R., Goldstein, A. H., Liu, S., Day, D. A., Russell, L. M., Rubitschun, C. L., Surratt, J. D., and Cohen, R. C.: Gas/particle partitioning of total alkyl nitrates observed with TD-LIF in Bakersfield J. Geophys. Res.-Atmos., 118, 6651–6662, doi:10.1002/jgrd.50522, 2013.

Russell, G. A.: Deuterium-isotope Effects in the Autoxidation of Aralkyl Hydrocarbons. Mechanism of the Interaction of Peroxy Radicals, J. Am. Cgem. Soc., 79, 3871–3877, doi:10.1021/ja01571a068, 1957.

Russell, M. and Allen, D. T.: Predicting secondary organic aerosol formation rates in southeast Texas, J. Geophys. Res.-Atmos., 110, D07S17, doi:10.1029/2004JD004722, 2005.

Sato, K.: Detection of nitrooxypolyols in secondary organic aerosol formed from the photooxidation of conjugated dienes under high-NOx conditions, Atmos. Environ., 42, 6851–6861, doi:10.1016/j.atmosenv.2008.05.010, 2008.

Saunders, S. M., Jenkin, M. E., Derwent, R. G., and Pilling, M. J.: Protocol for the development of the Master Chemical Mechanism, MCM v3 (Part A): tropospheric degradation of non-aromatic volatile organic compounds, Atmos. Chem. Phys., 3, 161–180, doi:10.5194/acp-3-161-2003, 2003.

Schichtel, B. A., Malm, W. C., Bench, G., Fallon, S., McDade, C. E., Chow, J. C., and Watson, J. G.: Fossil and contemporary fin particulate carbon fractions at 12 rural and urban sites in the United States, J. Geophys. Res.-Atmos., 113, D02311, doi:10.1029/2007JD008605, 2008.

Schröder, K., Junge, K., Spannenberg, A., and Beller, M.: Design of a bio-inspired imidazole-based iron catalyst for epoxidation of olefins Mechanistic insights, Catalysis Today, 157, 364–370, doi:10.1016/j.cattod.2010.04.034, 2010.

Slusher, D. L., Huey, L. G., Tanner, D. J., Flocke, F. M., and Roberts, J. M.: A thermal dissociation–chemical ionization mass spectrometry (TD-CIMS) technique for the simultaneous measurement of peroxyacyl nitrates and dinitrogen pentoxide, J. Geophys. Res.-Atmos., 109, D19315, doi:10.1029/2004JD004670, 2004.

Spittler, M., Barnes, I., Bejan, I., Brockmann, K. J., Benter, T., and Wirtz, K.: Reactions of NO_3 radicals with limonene and alpha-pinene: Product and SOA formation, Atmos. Environ., 40, S116–S127, doi:10.1016/j.atmosenv.2005.09.093, 2006.

Stockwell, C. E., Veres, P. R., Williams, J., and Yokelson, R. J.: Characterization of biomass burning emissions from cooking fires peat, crop residue, and other fuels with high-resolution proton-transfer-reaction time-of-fligh mass spectrometry, Atmos. Chem. Phys., 15, 845–865, doi:10.5194/acp-15-845-2015, 2015.

Stolle, A., Ondruschka, B., and Hopf, H.: Thermal Rearrangements of Monoterpenes and Monoterpenoids, Helvetica Chimica Acta, 92, 1673–1719, doi:10.1002/hlca.200900041, 2009.

Suarez-Bertoa, R., Picquet-Varrault, B., Tamas, W., Pangui, E., and Doussin, J. F.: Atmospheric Fate of a Series of Carbonyl Nitrates: Photolysis Frequencies and OH-Oxidation Rate Constants, Environ. Sci. Technol., 46, 12502–12509, doi:10.1021/es302613x, 2012.

Surratt, J. D., Lewandowski, M., Offenberg, J. H., Jaoui, M., Kleindienst, T. E., Edney, E. O., and Seinfeld, J. H.: Effect of Acidity on Secondary Organic Aerosol Formation from Isoprene, Environ. Sci. Technol., 41, 5363–5369, doi:10.1021/es0704176, 2007.

Szmigielski, R., Vermeylen, R., Dommen, J., Metzger, A., Maenhaut, W., Baltensperger, U., and Claeys, M.: The acid effect in the formation of 2-methyltetrols from the photooxidation of isoprene in the presence of NOx, Atmos. Res., 98, 183–189, doi:10.1016/j.atmosres.2010.02.012, 2010.

Thornton, J. A., Braban, C. F., and Abbatt, J. P. D.: N_2O_5 hydrolysis on sub-micron organic aerosols: the effect of relative humidity, particle phase, and particle size, Phys. Chem. Chem. Phys., 5, 4593–4603, doi:10.1039/B307498F, 2003.

Turrà, N., Neuenschwander, U., Baiker, A., Peeters, J., and Hermans, I.: Mechanism of the Catalytic Deperoxidation of tert-Butylhydroperoxide with Cobalt(II) Acetylacetonate, Chem.-Eur. J., 16, 13226–13235, doi:10.1002/chem.201000489, 2010.

Vereecken, L. and Peeters, J.: Nontraditional (Per)oxy Ring-Closure Paths in the Atmospheric Oxidation of Isoprene and Monoterpenes, J. Phys. Chem. A, 108, 5197–5204, doi:10.1021/jp049219g, 2004.

Vereecken, L. and Peeters, J.: A Theoretical Study of the OH-initiated Gas-phase Oxidation Mechanism of β-pinene ($C_{10}H_{16}$): First Generation Products, Phys. Chem. Chem. Phys., 14, 3802–3815, doi:10.1039/C2CP23711C, 2012.

Verma, V., Fang, T., Guo, H., King, L., Bates, J. T., Peltier, R. E., Edgerton, E., Russell, A. G., and Weber, R. J.: Reactive oxygen species associated with water-soluble $PM_{2.5}$ in the southeastern United States: spatiotemporal trends and source apportionment, Atmos. Chem. Phys., 14, 12915–12930, doi:10.5194/acp-14-12915-2014, 2014.

Wängberg, I., Barnes, I., and Becker, K. H.: Product and Mechanistic Study of the Reaction of NO_3 Radicals with α-Pinene, Environ. Sci. Technol., 31, 2130–2135, doi:10.1021/es960958n, 1997.

Wayne, R. P., Barnes, I., Biggs, P., Burrows, J. P., Canosamas, C. E., Hjorth, J., Lebras, G., Moortgat, G. K., Perner, D., Poulet, G., Restelli, G., and Sidebottom, H.: The nitrate radical – physics, chemistry, and the atmosphere, Atmos. Environ. Part a, 25, 1–203, doi:10.1016/0960-1686(91)90192-a, 1991.

Weber, R. J., Sullivan, A. P., Peltier, R. E., Russell, A., Yan, B., Zheng, M., de Gouw, J., Warneke, C., Brock, C., Holloway, J. S., Atlas, E. L., and Edgerton, E.: A study of secondary organic aerosol formation in the anthropogenic-influence southeastern United States, J. Geophys. Res.-Atmos., 112, D13302, doi:10.11029/12007JD008408, 2007.

Xu, H., Wentworth, P. J., Howell, N. W., and Joens, J. A.: Temperature Dependent Near-UV Molar Absorptivities of Aliphatic Aldehydes and Ketones in Aqueous Solution, Spectrochim. Acta A, 49, 1171–1178, doi:10.1016/0584-8539(93)80076-M, 1993.

Xu, L., Kollman, M. S., Song, C., Shilling, J. E., and Ng, N. L.: Effects of NOx on the Volatility of Secondary Organic Aerosol from Isoprene Photooxidation, Environ. Sci. Technol., 48, 2253–2262, doi:10.1021/es404842g, 2014.

Xu, L., Suresh, S., Guo, H., Weber, R. J., and Ng, N. L.: Aerosol characterization over the southeastern United States using high-resolution aerosol mass spectrometry: spatial and seasonal variation of aerosol composition and sources with a focus on organic nitrates, Atmos. Chem. Phys., 15, 7307–7336, doi:10.5194/acp-15-7307-2015, 2015a.

Xu, L., Guo, H., Boyd, C. M., Klein, M., Bougiatioti, A., Cerully, K. M., Hite, J. R., Isaacman-VanWertz, G., Kreisberg, N. M., Knote, C., Olson, K., Koss, A., Goldstein, A. H., Hering, S. V., de Gouw, J., Baumann, K., Lee, S.-H., Nenes, A., Weber, R. J., and Ng, N. L.: Effects of anthropogenic emissions on aerosol formation from isoprene and monoterpenes in the southeastern United States, Proc. Natl. Aca. Sci. USA, 112, 37–42, doi:10.1073/pnas.1417609112, 2015b.

Yeh, G. K. and Ziemann, P. J.: Alkyl Nitrate Formation from the Reactions of C8–C14 n-Alkanes with OH Radicals in the Presence of NOx: Measured Yields with Essential Corrections

for Gas–Wall Partitioning, J. Phys. Chem. A, 118, 8147–8157, doi:10.1021/jp500631v, 2014.

Yu, Y., Ezell, M. J., Zelenyuk, A., Imre, D., Alexander, L., Ortega, J., D'Anna, B., Harmon, C. W., Johnson, S. N., and Finlayson-Pitts, B. J.: Photooxidation of alpha-pinene at high relative humidity in the presence of increasing concentrations of NOx, Atmos. Environ., 42, 5044–5060, doi:10.1016/j.atmosenv.2008.02.026, 2008.

Zaveri, R. A., Berkowitz, C. M., Brechtel, F. J., Gilles, M. K., Hubbe, J. M., Jayne, J. T., Kleinman, L. I., Laskin, A., Madronich, S., Onasch, T. B., Pekour, M. S., Springston, S. R., Thornton, J. A., Tivanski, A. V., and Worsnop, D. R.: Nighttime chemical evolution of aerosol and trace gases in a power plant plume: Implications for secondary organic nitrate and organosulfate aerosol formation, NO_3 radical chemistry, and N_2O_5 heterogeneous hydrolysis, J. Geophys. Res.-Atmos., 115, D12304, doi:10.1029/2009jd013250, 2010.

Zhang, X., Cappa, C. D., Jathar, S. H., McVay, R. C., Ensberg, J. J., Kleeman, M. J., and Seinfeld, J. H.: Influenc of vapor wall loss in laboratory chambers on yields of secondary organic aerosol, Proc. Natl. Aca. Sci USA, 111, 5802-5807, doi:10.1073/pnas.1404727111, 2014.

Zhang, X., Schwantes, R. H., McVay, R. C., Lignell, H., Coggon, M. M., Flagan, R. C., and Seinfeld, J. H.: Vapor wall deposition in Teflo chambers, Atmos. Chem. Phys., 15, 4197–4214, doi:10.5194/acp-15-4197-2015, 2015.

Zhao, R., Lee, A. K. Y., and Abbatt, J. P. D.: Investigation of Aqueous-Phase Photooxidation of Glyoxal and Methylglyoxal by Aerosol Chemical Ionization Mass Spectrometry: Observation of Hydroxyhydroperoxide Formation, J. Phys. Chem. A, 116, 6253–6263, doi:10.1021/jp211528d, 2012.

Zheng, W., Flocke, F. M., Tyndall, G. S., Swanson, A., Orlando, J. J., Roberts, J. M., Huey, L. G., and Tanner, D. J.: Characterization of a thermal decomposition chemical ionization mass spectrometer for the measurement of peroxy acyl nitrates (PANs) in the atmosphere, Atmos. Chem. Phys., 11, 6529–6547, doi:10.5194/acp-11-6529-2011, 2011.

Ziemann, P. J. and Atkinson, R.: Kinetics, products, and mechanisms of secondary organic aerosol formation, Chem. Soc. Rev., 41, 6582–6605, doi:10.1039/c2cs35122f, 2012.